Article

Application of the FDTD Method to the Analysis of Electromagnetic Wave Propagation in Systems with Concrete and Reinforced Concrete

Agnieszka Choroszucho [1,*] **, Tomasz Szczegielniak** [2] **, Dariusz Kusiak** [2] **and Anna Jaskot** [3]

[1] Department of Electrical Engineering, Power Electronics and Power Engineering, Faculty of Electrical Engineering, Białystok University of Technology, Wiejska 45D Str., 15-351 Białystok, Poland

[2] Department of Automation, Electrical Engineering and Optoelectronics, Faculty of Electrical Engineering, Częstochowa University of Technology, Armii Krajowej 17, 42-200 Częstochowa, Poland; tomasz.szczegielniak@pcz.pl (T.S.); dariusz.kusiak@pcz.pl (D.K.)

[3] Department of Civil Engineering, Faculty of Civil Engineering, Częstochowa University of Technology, Akademicka 3, 42-200 Częstochowa, Poland; anna.jaskot@pcz.pl

* Correspondence: a.choroszucho@pb.edu.pl

Abstract: Wireless communication very often causes problems due to its quality. Problems with the network are very important when installing wireless networks inside buildings. The reason is the effects created during the propagation of electromagnetic waves inside rooms due to, among other factors, the construction of the walls and the building materials used. At the stage of network design, it is possible to use numerical methods, which allow for multivariate and fast analysis. This article presents a multivariate analysis of the impact of the variability in the electrical parameters of concrete and reinforced concrete on the propagation of electromagnetic waves and the value of the electric field intensity. The subject of the analysis was a wall composed of a homogeneous material (concrete) or non-homogeneous material (concrete with reinforcement). In the case of the homogeneous wall, the analysis was performed taking into account four electric permittivity values and a wide range of conductivity values. The analysis was performed at two frequencies used in wireless communication (2.4 GHz and 5 GHz). The analysis was performed using the time method based on Maxwell's equations—the finite difference time domain method (FDTD). The results of the numerical analysis were compared with the results obtained from the presented analytical relationships. In the next step, four models and calculations were obtained for systems with a reinforced concrete wall, taking into account the variability in the spacing between the bars, the diameter of the reinforcement and the number of rows of reinforcement. The analysis of complex systems was performed at a frequency of 2.4 GHz. The aim of the presented analysis was to check how the change in the value of the electric permittivity of concrete affects the values of the field intensity and its effect on the analysis of systems composed of concrete with reinforcement. In the case of concrete, it was observed that, for conductivity above 0.9 S/m, regardless of the electric permittivity, all characteristics had a similar course. For low concrete loss, the greatest differences in the electric field intensity were observed at a frequency of 2.4 GHz rather than at 5 GHz. On the other hand, the analysis of systems with reinforced concrete showed, among other aspects, that models with two rows of bars and spacing of 0.15 m, regardless of the reinforcement diameter, were characterized by lower values of the electric field intensity compared to the variants with one row of bars.

Keywords: electromagnetic wave propagation; building materials; reinforced concrete; FDTD; wireless communication systems

1. Introduction

Thanks to Wi-Fi technology, it is possible to use wireless Internet. Data transfer takes place via electromagnetic waves, which have a specific frequency. Modern routers

offer many network standards, including transferring information in two bands—2.4 and 5 GHz [1,2]. The 2.4 GHz frequency, in ideal conditions, allows transfer at a speed of up to 450 or 600 Mbps, while the 5 GHz band reaches up to 1300 Mbps. The maximum data transfer speed also depends on the Wi-Fi standard used by the router.

The 2.4 GHz band works flawlessly in ideal conditions. A problem that affects many users is interference occurring at this frequency. Many home devices use this band, such as wireless devices, Bluetooth tools, or microwave ovens. Wi-Fi connectivity is so common that there are often several private networks in a small area that interfere with each other. The 2.4 GHz frequency has been very common for many years—it is supported by all computers, laptops, and smartphones, including older ones [2]. Due to such great popularity, the band can be heavily loaded. Users using the 2.4 GHz Internet complain about delays, which make it difficult to watch movies in full HD quality, among other issues. Delays are particularly troublesome in apartment blocks, where many people usually use Wi-Fi channels at the same time. On the other hand, in single-family homes, there is much less interference due to the lack of neighbors.

The quality of wireless communication inside rooms is most influenced by the structure of the building, especially the walls. Due to the complex nature of the occurring physical phenomena (e.g., interference, reflections) and the variability in the geometry and composition of the material, it is necessary to consider models individually. The greatest problem is posed by walls composed of non-homogeneous materials such as hollow bricks or reinforced concrete. Wave propagation then has a changed wave front and multiple reflections occur. In the available literature, mainly homogeneous walls composed of solid bricks, concrete, and aerated concrete are analyzed [3,4]. In these publications, it can be noticed that the authors mainly focus on discussing material data and the values of the electrical parameters of the building materials, as well as the analysis of the attenuation coefficients of a given structure [3,5–8]. These are often theoretical rather than practical cases [7–9]. Table 1 presents the most significant studies related to the homogeneous material, i.e., concrete. On the other hand, Table 2 describes a complex material—reinforced concrete. Among others, based on these data and an additional review of the literature, information on the electrical parameters of concrete was collected (Table 3). As the results showed, there is large variability in the parameter values, which certainly affects the field values and wave propagation. However, many authors do not consider this and assume standard values, regardless of the frequency, type of concrete, w/c ratio, or concrete composition. In this study, a multivariate analysis was performed to check the extent to which changes in the values of the electrical parameters (i.e., electrical permittivity and conductivity) affect the values of the electric field. A very important element that determines the correct performance of calculations is the correct assignment of electrical parameter values to building materials. In the available publications, the authors analyze different thicknesses of concrete walls; they also check the effect of the angle of the wall in relation to the transmitter and determine coefficients, e.g., attenuation, but with arbitrarily entered material data.

More difficult in terms of application and more interesting due to the occurring field phenomena are issues related to structural elements containing reinforcements. The introduction of a metal into the wall causes the distortion of the propagating electromagnetic wave, which affects, among other aspects, the quality of wireless communication. The signal in a room behind a wall composed of a homogeneous material (e.g., concrete, brick) may have a value of three-quarters of the signal. On the other hand, walls composed of reinforced concrete may even result in a reduction in the signal to zero. The cause is steel rods, which reflect the signal; for this reason, there may be temporary signal loss or amplification. For this reason, research is being conducted on fiber concrete, which has metal particles and may meet construction requirements. Depending on the density of the metal particles used, effects that may be comparable to shielding are certainly possible. While maintaining the security of data capture, such a solution would be very welcome, but, from the point of view of Wi-Fi users, this would not be a suitable solution. For this

reason, detailed analyses of the impact of the amount of reinforcement and its diameter in the walls on the quality of communication are necessary in order to collect many data. This information could be a valuable source of knowledge when planning the positioning of the router and other elements included in the wireless network.

Table 1. Review of the latest important research related to concrete.

Frequency	Description	Literature
7–13 GHz	Analysis of the effect of the water/cement ratio in concrete on the values of the electrical permittivity of concrete. Samples of thickness 10.5–16.8 mm were tested for dry and wet concrete after 1 and 3 days from the time of production. The effect of the frequency of these samples on the attenuation was investigated. It was noticed that, at higher frequencies, the attenuation of the concrete layer increased rapidly. However, at lower frequencies (e.g., 5G technology), wetting the outer layer of a concrete wall caused additional signal attenuation of 6–12 dB. The relative permittivity was in the range of 4.89–10.25, while the thickness of the concrete plates was 10.5–16.8 mm.	[3]
2–62.4 GHz	A literature review on the applied values of electrical permittivity, including concrete. For example, for concrete at a frequency of 2 GHz, ε_r' is 5.81, and, at 5 GHz, $\varepsilon_r' = 5.5$. Very large discrepancies in this value at different frequencies were indicated.	[4]
33 GHz	A complex model of building materials was proposed to simulate the propagation of radio waves. The model was composed of multilayer plates (e.g., a 309-mm-thick concrete plate was tested, where the relative permittivity was 5.62).	[5]
1–6 GHz	An analysis of the dependence of the electrical permittivity of concrete on the thickness of the plate.	[10]
2–62 GHz	Testing the values of the electrical permittivity and conductivity without taking into account the variation in concrete thickness.	[11]
30–36 GHz	An analysis of the dependence of the electrical permittivity and conductivity on the plate thickness was performed.	[5]
0.2–67 GHz	Testing the values of the electrical permittivity and conductivity without taking into account the variation in concrete thickness.	[12]
200–500 GHz	Testing the values of the electrical permittivity and conductivity without taking into account the variation in concrete thickness.	[13]

Table 2. Review of conducted research related to reinforced concrete.

Description	Literature
Phenomena of electromagnetic field scattering by a metal grid placed in a perfect dielectric.	[7,14]
Analysis of a one-dimensional periodic row of conductive rods embedded inside a plate with dielectric properties, considering different angles of incidence of the electromagnetic wave. Single walls composed of reinforced concrete were analyzed.	[7,9,14]
Analysis of the impact of a reinforced concrete slab on radio communication; despite the wide frequency range of 0.1–6 GHz, it assumed constant homogenous material parameters of concrete determined at a frequency of 1 GHz.	[7]
The authors presented an analysis of a one-dimensional periodic row of conducting rods embedded inside a plate with dielectric properties, considering different angles of incidence of the electromagnetic wave.	[15]
A theoretical approach to metal meshes and their influence on the shielding efficiency is proposed.	[16]
Based on [16], single walls composed of reinforced concrete were modeled.	[7,9,14]
Analysis of concrete columns with reinforcement. Considered only for entire building structures.	[17]
Studies on the shielding properties of concrete doped with steel fibers. A non-destructive method was used, which eliminates the need to prepare samples with precise dimensions. A concrete slab with a reinforcing bar was also analyzed.	[18]
Analysis of non-destructive electromagnetic methods used in France to assess the condition of concrete and the durability of reinforced concrete structures.	[19]

Table 2. *Cont.*

Description	Literature
Modeling of the reflection and transmission of reinforced concrete using the Green's Moment and Function (MoM/GF) method for a wire mesh embedded in a dissipative dielectric plate. The angular dependence of the reflected and transmitted fields was investigated.	[20]
The calculation of the scattered wave through reinforced concrete walls modeled with a wire mesh is described. The MoM was used to find the wire currents.	[21]
The shielding properties of conductive concrete were studied in the 0–4 GHz range. An EM pulse in the form of a uniform plane wave was used.	[22]
At 2.5 GHz, an 80 mm × 80 mm model with one steel rod was analyzed. The steps and issues to be considered in 3D high-frequency simulation were presented.	[23]
Using FDTD, the UWB pulse propagation generated from a conical antenna through reinforced concrete building walls was checked. Analysis area 2.2 m × 2.2 m.	[24]
Using EM wave radar, an evaluation of the reinforcement and nodes between the crossings of bars was performed. Thanks to this method, it was possible to measure the diameters of the bars.	[25]

It should also be noted that the choice of numerical method imposes certain limitations, e.g., model size, simplifications with structure representation, homogenization of complex materials [26–30]. When using the ray tracing (RT) method, whole buildings are taken for analysis and often the electrical parameters of the materials have the same values regardless of the building materials and wall layering [2,30]. When using methods based on Maxwell's equations and model discretization, the problem is the size of the model [30,31]. Then, there must be a compromise between the exact representation of the model and the size of the analysis area. In this case, the authors apply the homogenization of the materials, e.g., they treat walls composed of bricks with hollows as full bricks [26].

As can be seen, homogeneous structures (concrete) have been analyzed by other authors. However, this concerned the determination of the reflection and attenuation coefficients and measurements of the electrical parameters of different types of concrete. There were no comparisons of the influence of the electrical parameters' variability on the electric field values. On this basis, it would be possible to determine how important arbitrary parameter assignment is in the analysis for, for example, concrete. This will be the basis for the further analysis of non-homogeneous materials (reinforced concrete). Knowing the influence of the variability—for example, in the electric permittivity of concrete—on the electric field, it would be possible to isolate the influence of the reinforcement layout and diameter on the quality of communication.

In the previous articles, systems with reinforcement were analyzed as single wall cases, without analyzing the variation in the number of reinforcement rows. The authors mainly considered non-invasive methods of reinforcement detection. In the case of checking the influence of steel bars on the transmission and reflection coefficients, grids with vertical and horizontal bars were rather considered. In these analyses, the influence of the substituted values of the electrical parameters of the concrete on the field values was not checked. A plate with an exemplary reinforcement grid arrangement was considered.

This article presents an analysis of the influence of the variability in the electrical parameters of concrete on the propagation of electromagnetic (EM) waves and the values of the electric field intensity. A 0.24 m-thick wall model was used for the analysis. In the case of concrete, two frequencies commonly used in wireless communication (2.4 GHz and 5 GHz) were used. A summary table reflecting the divergence of the electrical parameters of the concrete was also presented. The aim of this article is to demonstrate the influence of the variability in the electrical parameters for both concrete and reinforced concrete on the results. In the case of the analysis of composite materials (reinforced concrete), the article presents a multivariate analysis of the influence of the diameter of the bars (*fi*), the spacing between them (*L*) and the number of rows. In the case of this analysis, the frequency of 2.4 GHz was used. For selected cases, the instantaneous distributions of the electric field

are shown to observe the physical phenomena occurring in the considered systems with a wall composed of the considered building materials.

Section 2 describes the building materials used for the analysis (concrete and reinforced concrete). A summary table with the values of the electrical parameters describing concrete, which were used in the available publications, is also included. Section 3 briefly discusses other methods that are used to analyze the issues discussed in this article. The advantages and disadvantages of these methods are discussed. On this basis, the analysis methods that are also described (FDTD and analytical) are selected. Section 4 describes the analyzed models with a homogeneous material (concrete) and with a complex material (reinforced concrete). Section 5 presents the results and a discussion of the calculations performed. The propagation of the EM wave and the maximum values of the field intensity are presented. The influence of the variability in the electrical parameters on the field values in the case of concrete and reinforced concrete is checked. Section 6 highlights the most important conclusions from the analysis of EM wave propagation through a wall composed of concrete and reinforced concrete. The general conclusions from the detailed analysis of the considered building wall variants are provided at the end of this article.

2. Analyzed Building Materials

2.1. Concrete

Concrete is a heterogeneous and multiphase composite, mainly composed of cement, aggregates and water, which, after mixing, become a viscoelastic–solid body. This mixture, thanks to the hydration of the cement, changes into a solid body, whose properties constantly change during maturation. It is one of the most common building materials in modern construction. A concrete mix is a mixture of cement, aggregates, water and possible additives (up to 20% in relation to the mass of the binder) and admixtures (up to 5% in relation to the mass of the binder). The composition of the concrete mix is selected based on laboratory analyses and calculations (concrete formula), in order to obtain concrete with, e.g., appropriate abrasion, water resistance, acid resistance, heat resistance, and thermal insulation.

Most often, the quality of the concrete and the related changes in the values of the electrical parameters are reported in the literature. The authors in [32] showed that the real component of the electric permittivity of concrete (ε_r') reached a constant value after a month from the time of pouring, and the component value ε_r'' only did so after 14 months. Depending on the frequency, it is possible to find ε_r' in the range of 3–13 and conductivity from 0.0001 to 0.988 S/m. The typical electrical parameters of concrete are presented in Table 3.

Table 3. Electrical properties of concrete.

Frequency [GHz]	ε_r'	ε_r''	Conductivity [S/m]	Literature	Additional Information
10^{-6}–0.1	13	-	0.0001–0.02	[33]	Analysis of a slab composed of concrete and reinforcement
0.15–0.6	6	-	-	[34]	Analysis of different reinforcement densities in the slab
0.3–35.0	4.0–7.5	0.38–1.4	-	[35]	Analysis of the w/c coefficient variability
0.4–4.0	3	-	-	[36]	-

Table 3. *Cont.*

Frequency [GHz]	$\varepsilon_{\mathrm{r}}'$	$\varepsilon_{\mathrm{r}}''$	Conductivity [S/m]	Literature	Additional Information
0.5–2.0	6	0.01	-	[37]	-
0.5, 0.9, 1.0, 2.5	5.0–12.0	-	-	[38]	Data depending on concrete composition and frequency
0.8	7.1–7.5	-	-	[39]	Measurements for reinforced slab
0.9	6.26	-	0.037	[26]	Homogeneous concrete slab
0.948	5	-	0.004	[17]	Reinforced plate
1.0–2.0	6.07–5.87	-	0.0684–0.083	[40]	-
1.0–2.0	6	-	0.1	[40]	Data for concrete ceilings
1.0–3.0	3.0–6.0	-	$1.95 \cdot 10^{-3}$	[41]	Concrete wall analysis
0.1–6.0	6	-	$1.95 \cdot 10^{-3}$	[7]	-
1.5	6.398	-	0.182	[42]	-
1.5	5.113	-	0.031	[42]	-
1.5	6	-	0.01 (0.05 ÷ 0.25)	[42]	Tests with variability $\sigma = 0.05 \div 0.25$ S/m
1.8	6	-	$1.95 \cdot 10^{-3}$	[43]	-
1.8	7	0.3	-	[44]	Data for reinforced concrete, where, for steel, $\sigma = 1.11 \cdot 10^6$ S/m
1.8	6	-	$1.95 \cdot 10^{-3}$	[20]	Concrete with reinforcement referring to [1]
1.8	7	0.35	-	[14]	Homogeneous plate
1.865 2.14	5	-	0.004	[17]	Reinforced concrete
2.4	6	-	$1.95 \cdot 10^{-3}$	[45]	-
2.4	8	-	0.01	[45]	-
3	3	0.03	-	[44]	Concrete plate with holes
3.1–10.6	6	-	-	[34]	Reinforced concrete slab
5	5.5	-	0.0501	[4]	A wall composed of one-year-old concrete
5	4.6	-	0.0668	[46]	A wall composed of 40-year-old concrete
10	5.1	0.4	-	[4]	Dry concrete
10	6	1	-	[4]	Wet concrete
10.38	-	-	-	[47]	Graphs for ε' and $\varepsilon_{\mathrm{r}}''$
57.5	2.55	0.081	-	[48]	Dry concrete
57.5	6.5	0.43	-	[48]	-
60	6.4954	-	1.43	[46]	One-year-old concrete
60	11.47	-	0.988	[46]	Concrete slab

2.2. Structural Elements Composed of Reinforced Concrete

In reinforced concrete, stresses are transferred to the reinforcing bars, while the concrete supports the load induced in the entire structural element. Thanks to this, reinforced concrete is resistant to vibration and shock and can create a thin structure with a smaller

cross-section of the surface to support loads. The overall strength of concrete is increased by using various types of additives and reinforcements in the form of meshes, steel bars, and wires, which are embedded in the concrete before setting. Concrete reinforcement is commonly called reinforcement. The combination of these two materials creates a strong bond that is able to resist the action of both compressive and tensile forces. The nominal diameter of the steel bars (*fi*) is in the range of 0.005–0.04 m.

Reinforced concrete allows for the construction of a building structure of any shape and high durability. It is characterized by fire resistance and shows significant resistance to permanent and variable loads. Reinforced concrete is a structural composite that allows for the best use of the properties of the materials that constitute its composition: concrete is responsible for transferring compressive forces, while steel is responsible for tensile forces. Elements in the form of rods, ropes, strings, cables, and meshes are used to reinforce concrete, which allows for the transfer of much greater loads. However, it is not an ideal material, because reinforced concrete structures are heavy and, in practice, there is little possibility of changing the shape once it has been formed.

3. Analysis Methods Used

In the practice of engineers specializing in electronics, electrical engineering, telecommunications, or optics, knowledge of phenomena related to the propagation of electromagnetic waves plays an important role. It is important to master the mathematical apparatus that allows the completion of design tasks, as well as to intuitively understand electrodynamic phenomena and the operation of devices based on them. To achieve this goal, in addition to a theoretical description, the visualization of electromagnetic wave propagation in various conditions can be helpful.

In the generally available literature on radio wave propagation modeling methods, a number of solutions can be found, differing in terms of

- The modeled propagation environment (free space, urbanized area, building interiors);
- The dimensionality (two-dimensional, three-dimensional);
- The achievable calculation accuracy.

Only a few of them can be used to model radio wave propagation in anechoic chambers. Despite the development of numerical methods for the solution of electromagnetic problems, the creation of a software application to implement specific radio wave propagation models is still very difficult. A group of radio wave propagation modeling methods can be distinguished; with these, after certain simplifications, it is possible to obtain simulation results with acceptable accuracy in an acceptable duration. This group includes the ray tracing (RT) method. The phenomena of the transmission and reflection of radio waves cause significant difficulties in the unambiguous determination of the optical paths of the traced rays. Depending on the implementation, this method is based on the analysis of either only those rays that hit the receiving antenna directly or the additional analysis of reflected and refracted rays (adaptive method). Calculating the field intensity distribution using the RT method does not require the implementation of complex numerical methods. The use of ray tracing allows for a compromise between the speed of the algorithm and the accuracy of calculations.

The direct observation of many wave phenomena often requires expensive laboratory facilities and, in some cases, may be impossible. However, properly prepared simulations can supplement real experiments. Of particular interest is the method of solving Maxwell's equations in the time domain using finite differences—FDTD. It allows the visualization of the course of electromagnetic wave propagation in time, which makes it attractive as a scientific aid. The FDTD method is based on Maxwell's equations, which include the rotation of the electric and magnetic fields.

Wireless communication technologies consist of solutions that are differentiated in terms of their frequency or range of operation. Mobile radio communication systems can be distinguished, in which the range of base stations reaches kilometers, as well as local wireless communication systems, the task of which is to connect various parts of

the IT infrastructure within a building or room. From the point of view of modeling electromagnetic phenomena in these systems, the direct, relative measure of the size of the analyzed model should reflect the linear dimensions of the system in relation to the length of the propagating electromagnetic wave. The choice of the calculation method is largely dictated by the relative size of the model and the resulting approximations in the representation of physical phenomena.

The choice of a computational algorithm requires consideration of the needs and constraints related to the specificity of the analysis of field phenomena in wireless transmission systems. The fundamental factors determining the application of numerical simulation methods remain interdependent and are largely opposed in nature.

Physical conditions:

- The size of the modeled area in relation to the EM wavelength;
- The boundary conditions used in open-area mapping;
- The heterogeneity of the structures of building materials;
- The differentiation of material data (e.g., reinforcement);
- The operating ranges of base stations;
- The complexity of the geometry and terrain;
- Maintaining tolerances in building structures.

Numerical conditions:

- Errors in approximating the field distribution resulting from simplifications in the description of physical phenomena;
- The fidelity of geometric detail reproduction;
- No data for substitute parameters characterizing composite materials;
- The cost of performing calculations resulting from the complexity of the algorithm;
- The requirements of the calculation method due to the size of the data;
- The choice of a time or frequency method;
- The choice of an explicit or implicit method.

A classic example is the contradiction between increasing the size of the model and maintaining the expected precision of the material structure representation and the accuracy in modeling real systems. The contradictions of the indicated factors are emphasized when trying to analyze larger systems. The factor related to the numerical cost of the calculations also becomes important. The considered issues of EM wave propagation belong to the group of open problems. Despite the relatively small range of operation of local wireless communication systems (e.g., within buildings), the representation of field phenomena is associated with the reproduction of wave propagation phenomena in an open, theoretically infinite area. In local wireless communication systems, the boundaries of wave propagation are not limited to the building area; hence, the complexity and size of the considered area should be taken into account, and the boundary conditions that best reflect the modeled system should be adopted.

Issues related to the functioning of wireless networks and the distribution of the electromagnetic field require the consideration of many phenomena occurring during wave propagation in complex systems. For this purpose, in addition to empirical methods, the following methods can be used: analytical methods, using geometrical optics approximation (e.g., ray tracing techniques), and various numerical methods based on the solution of wave physics problems (e.g., FDTD, FDFD). The necessary approximations introduced during model construction and the errors introduced during the calculations are the main factors determining the choice of the calculation algorithm. The use of analytical methods leads to solutions that are fully based on the mathematical model and burdened with the smallest error. However, their use is only possible in systems with simple geometries [49,50]. The limitations of analytical methods do not allow the consideration of issues related to the propagation of electromagnetic waves in complex real building structures. Their use is limited to checking and comparing the approximate solution obtained using numerical methods, in the case of simple test models.

3.1. Methods of Geometrical Optics

Due to the considerable relative size of the models under consideration (reaching hundreds to thousands of wavelengths), geometrical optics methods have been widely used [6–8,30,31,44]. Assuming the rectilinear propagation of waves from the base station point, area coverage maps are determined, taking into account multiple reflections, partial wave refractions, and their attenuation. Virtual maps of the analyzed area, based on a vector representation of the terrain, buildings, and other obstacles, create the initial model for calculations. The analysis performed takes into account the multipath nature of the signal, which is subject to multiple reflections. However, the method of describing physical phenomena does not allow the consideration of wave interference. Limiting the error using this method requires the use of a large number of numerically modeled rays (even up to 40,000).

The main disadvantage of the RT method is the fact that the analysis of a complex, extensive area or complex geometry requires a large amount of computational time. This is caused by the increase in the number of interactions between rays and objects, which results in an exponential increase in the computational time. The formulations of other geometrical optics methods aim to extend the scope of their application, limit the disadvantages of the classical RT algorithm, or take into account additional phenomena in order to reduce the errors. Hence, modified geometrical optics algorithms are also discussed in the literature, including the energy method, uniform geometrical theory of diffraction (UTD) method, shooting and bouncing ray (SBR) method, and method of mirror images (image method) [8,30,31].

The RT method is suitable for modeling large areas, including urban environments [30]. To determine the wave reflection coefficient, authors often assume general electrical parameters for all types of building structures, e.g., $\varepsilon_r' = 5$, $\sigma = 0.01$ [S/m] [51]. RT-based methods are also used in the analysis of wave propagation in buildings, but within one floor inside the building. In [40], an extended two-story model was presented, taking into account walls and ceilings, as well as windows. In the case of non-homogeneous walls (including structures containing reinforcing bars or those composed of materials where the size of non-homogeneous spaces is comparable to the length of the electromagnetic wave), the above methods are unreliable and they require detailed analysis based on precise modeling [7].

3.2. Methods of Wave Physics

Wave physics methods are based on solving a model of a system described by Maxwell's equations. The most popular methods include FDTD and FEM. The essence of the indicated method is to create a discrete grid model of the tested object, consisting of elementary cells (called Yee cells), and to calculate instantaneous field distributions assuming the linear approximation of changes. This method is widespread, mainly due to the simplicity and accessibility of the formulation and the intuitive approach to solving Maxwell's equations [52–54]. In [42], the authors confirmed the agreement of the results obtained by the FDTD method with the values obtained using measurements. The authors' goal was to analyze a concrete slab depending on its roughness and the quality of the workmanship.

The finite element method (FEM) is also commonly used to analyze the discussed issues. Its advantage is the ability to create complex models of the systems under consideration by using adaptive meshes, which, among other aspects, allows for the representation of non-homogeneous materials, e.g., those containing cross-reinforcement. An example of the FEM method's application is presented in [14]. A concrete slab with a single layer of cross-reinforcement was analyzed. The authors determined the reflection and transmission coefficients for different angles of electromagnetic wave incidence as a function of the wall thickness (0.02–0.2 m), for both homogeneous concrete slabs and those containing a metal mesh inside the structure.

A separate group consists of hybrid methods, which combine analytical and numerical methods or various numerical methods. The proposed solutions aim to consider models with complex geometries or increase the area subject to modeling [43,55]. This paper presents a hybrid algorithm based on MoM, which allowed for the analysis of reinforcement bar systems forming cages. The properties of the base material, i.e., the surrounding concrete, were omitted. An increasingly frequently used method to develop new hybrid methods is FDTD. For example, in [30], a method equivalent to the ray tracing method (multiple-ray method) using the FDTD algorithm was presented. The aim of adopting such a method was to integrate the calculation of propagation models based on geometrical optics, in both large open models covering several buildings and inside buildings. In [26], the authors used a hybrid method based on RT to analyze the shielding effectiveness. They showed that the proposed method was less time-consuming compared to FEM and allowed for the estimation of the transmission coefficient value. Hybrid methods are not without their drawbacks, and modifications and combinations of different methods for the calculation of field distributions inside complex rooms are still being examined.

In [27,30,31,56,57], the effectiveness and usefulness of such methods regarding the discussed issues are discussed. An example is [30], in which the results obtained by the FDTD and RT methods were compared. The results were convergent only when the number of rays used in RT was in the order of 181 and when the distance from the window was at least fifteen times greater than the wavelength. The calculation results showed that methods based on wave physics are characterized by greater flexibility in modeling structures and realistically reflect the phenomena occurring inside building structures. Moreover, in [31], the authors proved the convergence of the results between the method based on ray tracing and FDTD using the example of simple models of homogeneous walls. On the other hand, it was found that the FDTD method allowed for a more accurate analysis of various types of walls (e.g., reinforced concrete).

In the case of the frequency-based method (FDFD), the resulting description of the model under consideration is obtained by combining differential dependencies created for each grid node. In the final notation, a matrix equation is obtained, where $\underline{\mathbf{A}}$ denotes the complex matrix of coefficients. In the general case, the matrix $\underline{\mathbf{A}}$ is non-singular (det $\underline{\mathbf{A}} \neq 0$) and asymmetric. The size of the matrix, depending on the number of degrees of freedom (N_{DOF}) dim $\underline{\mathbf{A}} = N_{\text{DOF}} \cdot N_{\text{DOF}}$, excludes its full description within the algorithm. The constructed matrix is sparse, with the number of non-zero factors being at least $5 N_{\text{DOF}}$. Due to the properties of the $\underline{\mathbf{A}}$ and N_{DOF} matrices describing the model, special iterative methods and matrix packing, e.g., using the compressed row storage (CRS) technique, are necessary to determine the solution.

Due to its formulation, the frequency algorithm (FDFD) leads to the direct determination of the field distribution in the steady state. This algorithm is an implicit scheme but is unconditionally stable. The main limitation in its implementation is the construction and execution of calculations for models described in the domain of complex numbers. On the other hand, the time algorithm (FDTD) is an explicit scheme in which the representation of the model is reduced to a matrix description of the distribution of the materials in the model area. This set is sequentially searched in each step of the time scheme. The calculated field value is a linear combination of the appropriate factors, determined in earlier iterations over time. The determination of the field value using the FDTD scheme requires the calculation of the unsteady state at the beginning. To determine the distribution of the field intensity amplitude (the so-called envelope), it is also necessary to perform a sequence of calculations in the time domain after reaching the steady state.

The following factors affect the errors in calculations using the differential method:

- The mesh size of the grid discretizing the region where the solution is approximated by linear functions;
- The construction of the mesh discretizing the area, including possible local changes in its distribution related to the change in the mesh size;

- The limitations of the method resulting from the requirement for a cuboid (rectangular) mesh, which leads to the less accurate representation of irregular surfaces, e.g., rounded surfaces;
- The simplification of the representation of the real model;
- Imperfect spatial confinement by absorption boundary conditions, which, in the case of Mur's boundary conditions, requires the use of first-order differential approximations; therefore, the resultant order of approximations in the model is subject to local changes.

Taking into account the above method descriptions, the FDTD method was used for a multivariate analysis. In order to verify the results, the analytical method and FEM were also used.

3.3. FDTD Method Description

The FDTD method was used to determine the electromagnetic field distribution in the analyzed model [52]. It is useful in calculating time-varying electromagnetic fields for high-frequency and broadband signals. Maxwell's curl equations in time and space are the basis of the FDTD method [52,53]:

$$\nabla \times \mathbf{E} = -\frac{\partial \mathbf{B}}{\partial t}, \tag{1}$$

$$\nabla \times \mathbf{H} = \sigma \mathbf{E} + \frac{\partial \mathbf{D}}{\partial t} + \mathbf{J}_I, \tag{2}$$

where **E**—the electric field, **H**—the magnetic field, $\mathbf{J}_I$—the current density vector. The description of the problems using Equations (1) and (2) permits us to determine the field distribution in the unsteady state, as well as in the steady state. After applying decomposition, Equations (1) and (2) are introduced as six coupled first-order differential equations that describe the components of **E** and **H**:

$$\frac{\partial E_x}{\partial t} = \frac{1}{\varepsilon} \left(\frac{\partial H_z}{\partial y} - \frac{\partial H_y}{\partial z} - \sigma E_x \right), \tag{3}$$

$$\frac{\partial E_y}{\partial t} = \frac{1}{\varepsilon} \left(\frac{\partial H_x}{\partial z} - \frac{\partial H_z}{\partial x} - \sigma E_y \right), \tag{4}$$

$$\frac{\partial E_z}{\partial t} = \frac{1}{\varepsilon} \left(\frac{\partial H_y}{\partial x} - \frac{\partial H_x}{\partial y} - \sigma E_z \right), \tag{5}$$

$$\frac{\partial H_x}{\partial t} = \frac{1}{\mu} \left(\frac{\partial E_y}{\partial z} - \frac{\partial E_z}{\partial y} \right), \tag{6}$$

$$\frac{\partial H_y}{\partial t} = \frac{1}{\mu} \left(\frac{\partial E_z}{\partial x} - \frac{\partial E_x}{\partial z} \right), \tag{7}$$

$$\frac{\partial H_z}{\partial t} = \frac{1}{\mu} \left(\frac{\partial E_x}{\partial y} - \frac{\partial E_y}{\partial x} \right). \tag{8}$$

In the developed formulation of the differential method in the frequency domain, a construction with a shifted grid for the electric and magnetic field components was adopted. The grid structure reflects the physical interpretation of electromagnetic phenomena and is consistent with the concept proposed by K. S. Yee in the formulation of the differential method in the time domain [52]. The construction of Yee's elementary cell takes the form presented in Figure 1a. The determined spatial distributions of the physical quantities $\{E_x,$ $E_y, E_z, H_x, H_y, H_z\}$ are assigned at selected points in the area (x, y, z), taking into account a discrete, finite size for the integration step over the area $(\Delta_x, \Delta_y, \Delta_z)$. Each component of the electric field intensity vector is surrounded by the corresponding components of the magnetic field intensity vector rotating around it. In the case of the **H** vector components, the notation is analogous. In the two-dimensional model, however, the development of

the scheme is based on the construction of a rectangular grid with a shifted **E** and **H** (Figure 1b). In a two-dimensional system, for example, the description TM$_z$ means that the magnetic field components H_x and H_y are described in the model plane, and the E_z vector is perpendicular to the distinguished direction.
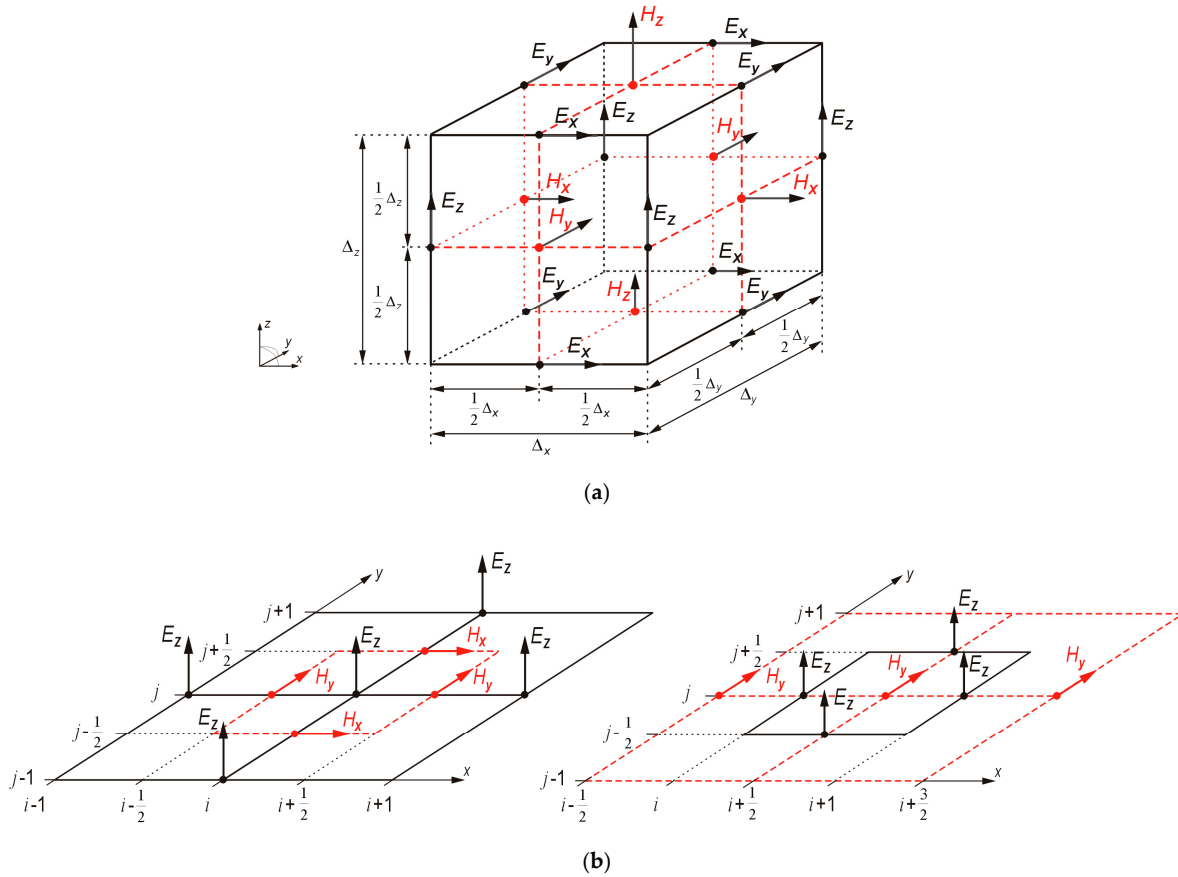

(**a**)

(**b**)

Figure 1. Discretization of Maxwell's equations for the region: (**a**) three-dimensional, (**b**) two-dimensional (TMz variant) with consideration of a shifted differential grid.

The components of the EM field are calculated at different points in space. The iterative integration of Maxwell's equations is based on the use of a two-step scheme. In choosing steps *n*, the electric field distribution is determined, while the values of the components of **H** are calculated from the displacement at the moment Δ_t. Applying Euler's scheme of central differences to the approximation of the partial derivatives, Equations (3)–(8) take the following structure:

$$\frac{\overset{n+1}{i,j,k}E_x - \overset{n}{i,j,k}E_x}{\Delta_t} = \frac{1}{\varepsilon_{i,j,k}}\left(\frac{\overset{n+\frac{1}{2}}{i,j+\frac{1}{2},k}H_z - \overset{n+\frac{1}{2}}{i,j-\frac{1}{2},k}H_z}{\Delta_y} - \frac{\overset{n+\frac{1}{2}}{i,j,k+\frac{1}{2}}H_y - \overset{n+\frac{1}{2}}{i,j,k-\frac{1}{2}}H_y}{\Delta_z} - \sigma_{i,j,k}\overset{n+\frac{1}{2}}{i,j,k}E_x\right), \tag{9}$$

$$\frac{\overset{n+1}{i,j,k}E_y - \overset{n}{i,j,k}E_y}{\Delta_t} = \frac{1}{\varepsilon_{i,j,k}}\left(\frac{\overset{n+\frac{1}{2}}{i,j,k+\frac{1}{2}}H_x - \overset{n+\frac{1}{2}}{i,j,k-\frac{1}{2}}H_x}{\Delta_z} - \frac{\overset{n+\frac{1}{2}}{i+\frac{1}{2},j,k}H_z - \overset{n+\frac{1}{2}}{i-\frac{1}{2},j,k}H_z}{\Delta_x} - \sigma_{i,j,k}\overset{n+\frac{1}{2}}{i,j,k}E_y\right), \tag{10}$$

$$\frac{\overset{n+1}{i,j,k}E_z - \overset{n}{i,j,k}E_z}{\Delta_t} = \frac{1}{\varepsilon_{i,j,k}}\left(\frac{\overset{n+\frac{1}{2}}{i+\frac{1}{2},j,k}H_y - \overset{n+\frac{1}{2}}{i-\frac{1}{2},j,k}H_y}{\Delta_x} - \frac{\overset{n+\frac{1}{2}}{i,j+\frac{1}{2},k}H_x - \overset{n+\frac{1}{2}}{i,j-\frac{1}{2},k}H_x}{\Delta_y} - \sigma_{i,j,k}\overset{n+\frac{1}{2}}{i,j,k}E_z\right), \tag{11}$$

$$\frac{_{i,j,k}^{n+\frac{1}{2}}H_x - _{i,j,k}^{n-\frac{1}{2}}H_x}{\Delta_t} = \frac{1}{\mu_{i,j,k}}\left(\frac{_{i,j,k+\frac{1}{2}}^{n}E_y - _{i,j,k-\frac{1}{2}}^{n}E_y}{\Delta_z} - \frac{_{i,j+\frac{1}{2},k}^{n}E_z - _{i,j-\frac{1}{2},k}^{n}E_z}{\Delta_y}\right), \tag{12}$$

$$\frac{_{i,j,k}^{n+\frac{1}{2}}H_y - _{i,j,k}^{n-\frac{1}{2}}H_y}{\Delta_t} = \frac{1}{\mu_{i,j,k}}\left(\frac{_{i+\frac{1}{2},j,k}^{n}E_z - _{i-\frac{1}{2},j,k}^{n}E_z}{\Delta_x} - \frac{_{i,j,k+\frac{1}{2}}^{n}E_x - _{i,j,k-\frac{1}{2}}^{n}E_x}{\Delta_z}\right), \tag{13}$$

$$\frac{_{i,j,k}^{n+\frac{1}{2}}H_z - _{i,j,k}^{n-\frac{1}{2}}H_z}{\Delta_t} = \frac{1}{\mu_{i,j,k}}\left(\frac{_{i,j+\frac{1}{2},k}^{n}E_x - _{i,j-\frac{1}{2},k}^{n}E_x}{\Delta_y} - \frac{_{i+\frac{1}{2},j,k}^{n}E_y - _{i-\frac{1}{2},j,k}^{n}E_y}{\Delta_x}\right). \tag{14}$$

The values $_{i,j,k}^{n+\frac{1}{2}}E$ are approximated:

$$_{i,j,k}^{n+\frac{1}{2}}E_z = \frac{_{i,j,k}^{n+1}E_z + _{i,j,k}^{n}E_z}{2} \tag{15}$$

By substituting Equation (15) into Equation (11), we obtain Equation (16). In order to illustrate the determination of the E_z component, a graphical interpretation of the equation is presented in Figure 2. To find the $_{i,j,k}^{n+1}E_z$ at step $n + 1$, it is essential to refer to the value of **H** (H_x, H_y) at time $n + 1/2$ and to the $_{i,j,k}^{n}E_z$.

$$_{i,j,k}^{n+1}E_z = \frac{1 - \frac{\sigma_{i,j,k}\Delta_t}{2\varepsilon_{i,j,k}}}{1 + \frac{\sigma_{i,j,k}\Delta_t}{2\varepsilon_{i,j,k}}} \cdot _{i,j,k}^{n}E_z + \frac{\frac{\Delta_t}{\varepsilon_{i,j,k}}}{1 + \frac{\sigma_{i,j,k}\Delta_t}{2\varepsilon_{i,j,k}}} \cdot \left(\frac{_{i+\frac{1}{2},j,k}^{n+\frac{1}{2}}H_y - _{i-\frac{1}{2},j,k}^{n+\frac{1}{2}}H_y}{\Delta_x} - \frac{_{i,j+\frac{1}{2},k}^{n+\frac{1}{2}}H_x - _{i,j-\frac{1}{2},k}^{n+\frac{1}{2}}H_x}{\Delta_y}\right), \tag{16}$$

where

$_{i,j,k}^{n+1}E_z$—the calculated value of the component along the *Oz* axis of the electric field intensity (E_z) at the observation point (*i,j,k*) in time ($n + 1$) based on the knowledge of the electromagnetic field components at the preceding moments Δ_t, at the appropriate points in space;

$_{i+\frac{1}{2},j,k}^{n+\frac{1}{2}}H_x$—the value of the component along the *Ox* axis of the magnetic field (H_x) at the observation point ($i + 1/2,j,k$) in time ($n + 1/2$);

$_{i-\frac{1}{2},j,k}^{n+\frac{1}{2}}H_x$—the value of the component along the *Ox* axis of the magnetic field (H_x) at the observation point ($i - 1/2,j,k$) in time ($n + 1/2$);

$_{i,j+\frac{1}{2},k}^{n+\frac{1}{2}}H_y$—the value of the component along the *Oy* axis of the magnetic field (H_y) at the observation point ($i, j + 1/2,k$) in time ($n + 1/2$);

$_{i,j-\frac{1}{2},k}^{n+\frac{1}{2}}H_y$—the value of the component along the *Oy* axis of the magnetic field (H_y) at the observation point ($i, j - 1/2,k$) in time ($n + 1/2$);

Δ_x—the discrete integration step size along the axis *Ox*;

Δ_y—the discrete integration step size along the axis *Oy*;

$\sigma_{i,j,k}$—the conductivity value at point (i, j, k);

$\varepsilon_{i,j,k}$—the value of the electrical permittivity at point (i, j, k).

Defining the coefficients, e.g., (17)–(19), allows for a simpler means of writing the difference equations:

$$c_{i,j,k}^{ee} = \frac{\varepsilon_{i,j,k} - \sigma_{i,j,k}\Delta_t}{\varepsilon i, j, k + \sigma_{i,j,k}\Delta_t}, \tag{17}$$

$$c_{i,j,k}^{ehy} = \frac{2\Delta_t}{2\varepsilon_{i,j,k} + \sigma_{i,j,k}\Delta_t} \cdot \frac{1}{\Delta_x}, \tag{18}$$

$$c_{i,j,k}^{ehx} = \frac{2\Delta_t}{2\varepsilon_{i,j,k} + \sigma_{i,j,k}\Delta_t} \cdot \frac{1}{\Delta_y}. \tag{19}$$
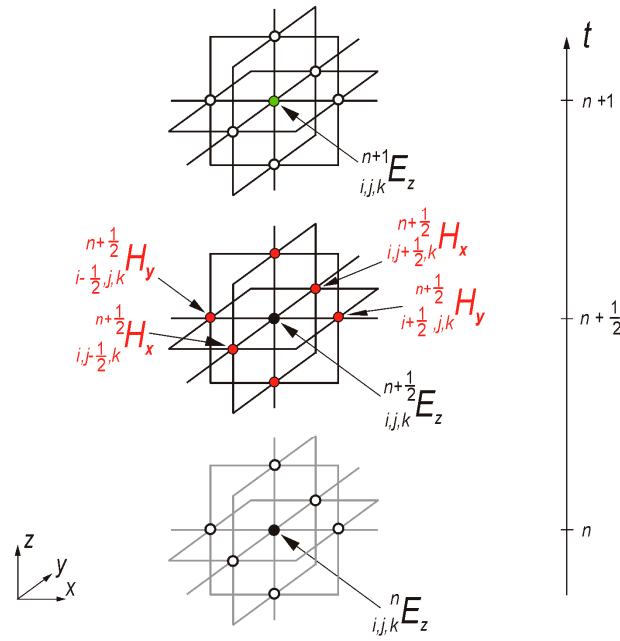
Figure 2. Determination of the values of the E_z components in step $n+1$ for the Yee cell with indices i, j, k.

Replacement coefficients are also introduced to depict the equations of the magnetic field components:

$$c_{i,j,k}^{hh} = \frac{2\,\mu_{i,j,k} - \Delta_t}{2\,\mu_{i,j,k} + \Delta_t}, \tag{20}$$

$$c_{i,j,k}^{hey} = \frac{\Delta_t}{\mu_{i,j,k}} \cdot \frac{1}{\Delta_x}, \tag{21}$$

$$c_{i,j,k}^{hex} = \frac{\Delta_t}{\mu_{i,j,k}} \cdot \frac{1}{\Delta_y}. \tag{22}$$

Assuming that $\Delta = \Delta_x = \Delta_y = \Delta_z$, we obtain

$$c_{i,j,k}^{eh} = c_{i,j,k}^{ehx} = c_{i,j,k}^{ehy} = c_{i,j,k}^{ehz}, \tag{23}$$

$$c_{i,j,k}^{he} = c_{i,j,k}^{hex} = c_{i,j,k}^{hey} = c_{i,j,k}^{hez}. \tag{24}$$

The applied coefficients allow for the easier notation of differential equations:

$$_{i,j,k}^{n+1}E_x = c_{i,j,k}^{ee} \cdot {}_{i,j,k}^{n}E_x + c_{i,j,k}^{eh} \cdot \left({}_{i,j+\frac{1}{2},k}^{n+\frac{1}{2}}H_z - {}_{i,j-\frac{1}{2},k}^{n+\frac{1}{2}}H_z - {}_{i,j,k+\frac{1}{2}}^{n+\frac{1}{2}}H_y + {}_{i,j,k-\frac{1}{2}}^{n+\frac{1}{2}}H_y \right), \tag{25}$$

$$_{i,j,k}^{n+1}E_y = c_{i,j,k}^{ee} \cdot {}_{i,j,k}^{n}E_y + c_{i,j,k}^{eh} \cdot \left({}_{i,j,k+\frac{1}{2}}^{n+\frac{1}{2}}H_x - {}_{i,j,k-\frac{1}{2}}^{n+\frac{1}{2}}H_x - {}_{i+\frac{1}{2},j,k}^{n+\frac{1}{2}}H_z + {}_{i-\frac{1}{2},j,k}^{n+\frac{1}{2}}H_z \right), \tag{26}$$

$$_{i,j,k}^{n+1}E_z = c_{i,j,k}^{ee} \cdot {}_{i,j,k}^{n}E_z + c_{i,j,k}^{eh} \cdot \left({}_{i+\frac{1}{2},j,k}^{n+\frac{1}{2}}H_y - {}_{i-\frac{1}{2},j,k}^{n+\frac{1}{2}}H_y - {}_{i,j+\frac{1}{2},k}^{n+\frac{1}{2}}H_x + {}_{i,j-\frac{1}{2},k}^{n+\frac{1}{2}}H_x \right), \tag{27}$$

$$_{i,j,k}^{n+\frac{1}{2}}H_x = c_{i,j,k}^{hh} \cdot {}_{i,j,k}^{n-\frac{1}{2}}H_x + c_{i,j,k}^{he} \cdot \left({}_{i,j,k+\frac{1}{2}}^{n}E_y - {}_{i,j,k-\frac{1}{2}}^{n}E_y - {}_{i,j+\frac{1}{2},k}^{n}E_z + {}_{i,j-\frac{1}{2},k}^{n}E_z \right), \tag{28}$$

$$_{i,j,k}^{n+\frac{1}{2}}H_y = c_{i,j,k}^{hh} \cdot {}_{i,j,k}^{n-\frac{1}{2}}H_y + c_{i,j,k}^{he} \cdot \left({}_{i+\frac{1}{2},j,k}^{n}E_z - {}_{i-\frac{1}{2},j,k}^{n}E_z - {}_{i,j,k+\frac{1}{2}}^{n}E_x + {}_{i,j,k-\frac{1}{2}}^{n}E_x \right), \tag{29}$$

$$_{i,j,k}^{n+\frac{1}{2}}H_z = c_{i,j,k}^{hh} \cdot {}_{i,j,k}^{n-\frac{1}{2}}H_z + c_{i,j,k}^{he} \cdot \left({}_{i,j+\frac{1}{2},k}^{n}E_x - {}_{i,j-\frac{1}{2},k}^{n}E_x - {}_{i+\frac{1}{2},j,k}^{n}E_y + {}_{i-\frac{1}{2},j,k}^{n}E_y \right). \tag{30}$$

The final equations show that the description of the algorithm leads to an explicit scheme. In this case, the matrix **A** is not built. Only by creating the table with $\{c_{i,j,k}^{ee}, c_{i,j,k}^{ehx},$ $c_{i,j,k}^{ehy}, c_{i,j,k}^{ehz}, c_{i,j,k}^{hh}, c_{i,j,k}^{hex}, c_{i,j,k}^{hey}, c_{i,j,k}^{hez}\}$ can we describe the individual Yee cells.

3.4. Analytical Solution

In order to verify the results, the analytical method described in [49,50] was used. The dependencies apply to homogeneous materials. The perpendicular incidence of the wave on the wall was taken into account. This corresponds to the problem of the propagation of a plane wave in an open space and its interaction with a plate composed of a dielectric [49,50]. Due to the harmonic dependence of the fields on time, the electric field vectors of the incident wave E_{1+}, the transmitted E_{1+}', and the reflected E_{1-} are written in complex form. The test system from Figure 3, in which the wall is a homogeneous material, is reduced to a one-dimensional layered model, in which the region of a homogeneous, isotropic dissipative dielectric Ω_{con} of the width b is surrounded by air.
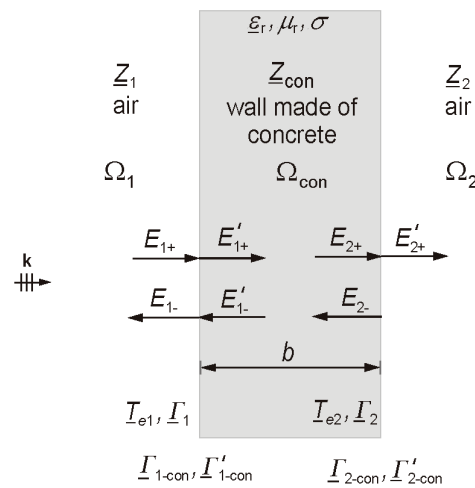
Figure 3. Perpendicular incidence of the EM wave on the concrete wall.

The characteristics of the surrounding air (1 and 2) are described by the wave impedance:

$$\underline{Z}_1 = \underline{Z}_2 = Z_0 = \sqrt{\frac{\mu_0}{\varepsilon_0}} \approx 377 \ \Omega. \tag{31}$$

The homogeneous building materials under consideration are categorized as non-ideal, low-loss dielectrics. Taking into account the effective permittivity of the dissipative dielectric, its wave impedance is represented by

$$\underline{Z}_{\mathrm{con}} = \sqrt{\frac{\mu}{\underline{\varepsilon}}} = \sqrt{\frac{\mu}{\varepsilon_r' - j\left(\frac{\sigma}{\omega} + \varepsilon_r''\right)}} = \sqrt{\frac{\mu_0 \, \mu_r}{\varepsilon_0 \, \varepsilon_r'}} \cdot \left(1 + j\left(\frac{\sigma + 2\pi \, f \cdot (\varepsilon_0 \, \varepsilon_r'')}{2 \cdot (2\pi \, f \cdot (\varepsilon_0 \, \varepsilon_r'))}\right)\right). \tag{32}$$

At the perpendicular incidence of a wave on the material boundary, the transmission coefficient of the electric field behind the dielectric is represented by Equation (32), where $\underline{k}$ is the wave number and $\underline{T}_{e1}$ and $\underline{T}_{e2}$ are the field coefficients in the first and second regions, respectively, where the values of air are assigned as

$$\underline{T}_e = |\underline{T}_e| = \left|\frac{E_{2+}'}{E_{1+}}\right| = \left|\frac{\underline{T}_{e1} \cdot \underline{T}_{e2} \cdot e^{-j\,\underline{k}b}}{1 + \underline{\Gamma}_1 \cdot \underline{\Gamma}_2 \cdot e^{-2j\,\underline{k}b}}\right| \tag{33}$$

The dependence in (32) allows for the verification of the results obtained during numerical calculations using the FDTD method. The obtained maximum values of the field

intensity behind the concrete are the basis for the determination of the field transmission coefficient directly, based on the definition in Equation (32).

4. Description of the Models Considered

Due to the construction of the walls and their geometry, a separate analysis of the phenomena was carried out for

- Homogeneous materials, namely concrete;
- Heterogeneous materials, namely concrete with steel bars (reinforced concrete).

The work carried out was aimed at assessing the phenomena occurring inside the structure. The influence of the electrical parameters of the material and the construction on the field distribution at the frequencies used in Wi-Fi wireless networks was examined.

The focus of the analysis was a wall composed of a concrete (thickness: 0.24 m). On both sides of the wall, there was air. Other factors that could interfere with EM wave propagation were not taken into account. The different percentages of the individual components of the concrete and the variability in the electrical parameters of the material meant that many variants were analyzed. The values of $\varepsilon_{r'} \in \{5, 6, 7, 8\}$ and $\sigma \in \langle 0, 0.3 \rangle$ S/m were adopted for analysis. Table 4 lists the dimensions of the structures under consideration in relation to the wavelength in concrete λ_c.

Table 4. Electrical dimensions of the considered wall models.

Relative Permittivity ε_{r}'	Wall Thickness	
	f = 2.4 GHz	*f* = 5 GHz
5	4.29 λ_c	8.95 λ_c
6	4.71 λ_c	9.79 λ_c
7	5.08 λ_c	10.57 λ_c
8	5.43 λ_c	11.32 λ_c

After analyzing the influence of the values of the electrical parameters of the concrete on the propagation of the EM wave and the values of the field intensity, calculations were performed for the composite material. In this case, a wall composed of concrete with a thickness of 0.24 m and four reinforcement variants were considered (Figure 4).
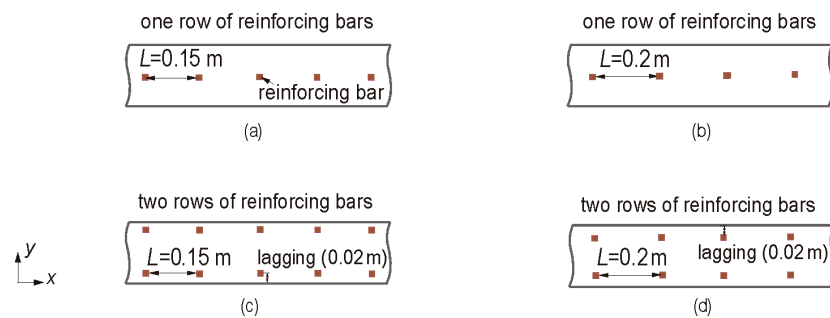

Figure 4. Variants of reinforced concrete walls: (**a**) 1b_L15, (**b**) 1b_L20, (**c**) 2b_L15, (**d**) 2b_L20.

- 1b_L15: one row of reinforcing bars and spacing $L = 0.15$ m;
- 1b_L20: $L = 0.2$ m and one row of bars;
- 2b_L15: two rows of reinforcing bars, $L = 0.15$ m;
- 2b_L20: two rows of bars, $L = 0.2$ m.

In every model, four values of the reinforcement diameter were considered: $fi \in \{0.006, 0.008, 0.01, 0.012\}$ m.

Based on the discussion of the walls composed of concrete (Section 2), the analysis also adopted $\varepsilon_{r}' \in \{5, 6, 7, 8\}$, as used in the literature. The variation in the electric field value

was considered depending on the selected conductivity, $\sigma \in \{0.00195, 0.004, 0.01\}$ S/m. The dimensions of the considered wall structure, in relation to the wavelength in concrete λ_c, at the frequency $f = 2.4$ GHz, are presented in Table 4.

5. Results of the Analysis

Thanks to the FDTD method, it was possible to obtain momentary images of the field (e.g., Figure 5). The maximum values of the E_z component (e.g., Figure 6) were obtained by developing a new algorithm to determine the largest field values from any number of momentary result files.
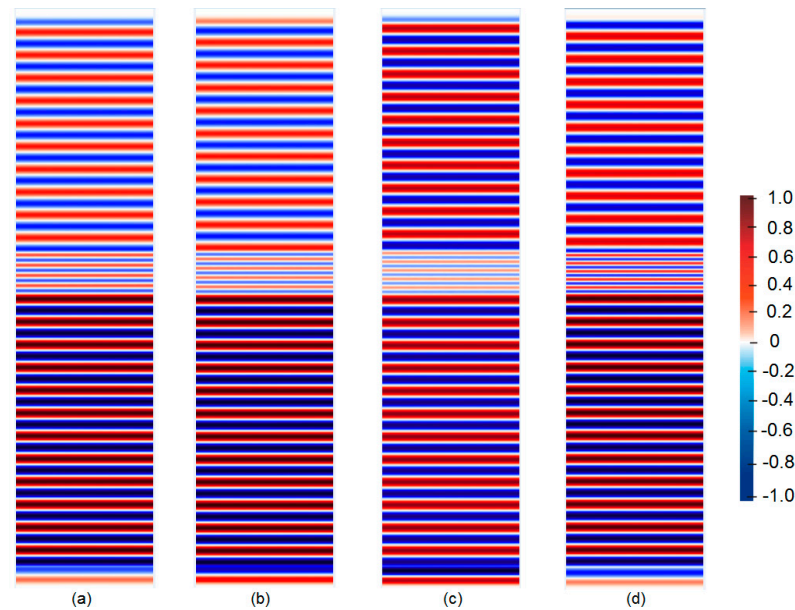
Figure 5. Comparison of the instantaneous distributions of the electric field intensity in the analyzed area with a wall of $\sigma = 0.00195$ S/m: (**a**) $\varepsilon_r' = 5$, (**b**) $\varepsilon_r' = 6$, (**c**) $\varepsilon_r' = 7$, (**d**) $\varepsilon_r' = 8$.
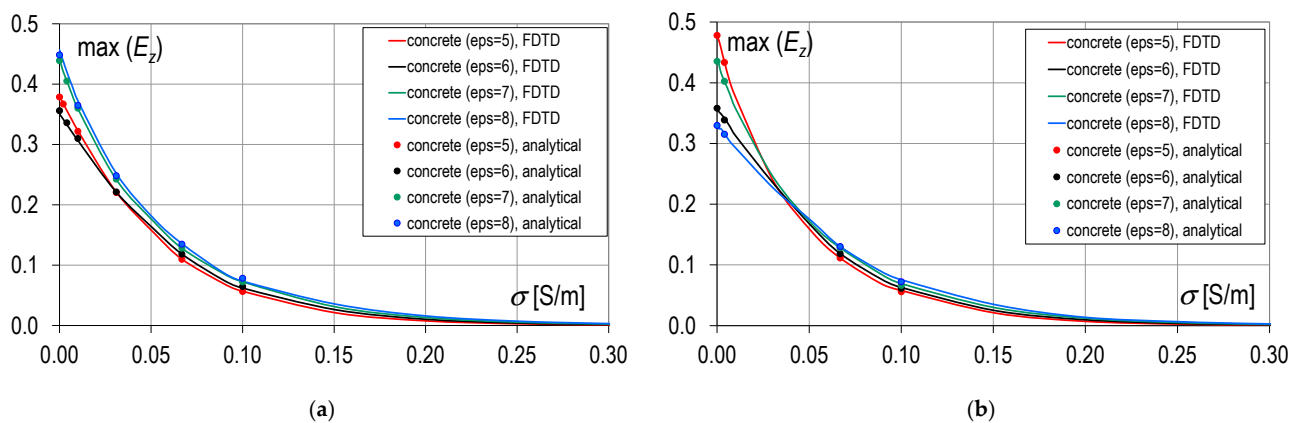
Figure 6. Maximum values of the E_z component behind a wall composed of concrete: (**a**) 2.4 GHz, (**b**) 5 GHz.

5.1. Analysis of the Influence of Concrete's Electrical Parameters on the Electric Field Intensity Values

The effect of variations in the electrical parameters of the concrete on the electric field intensity values is shown in Figure 6. The values of max(E_z) obtained by the numerical method were also verified using the analytical method (Section 3.2). The results of the analytical calculations are marked with points on the graphs. In addition, in order to verify the results, a test model of a concrete wall was performed in the Comsol Multiphysics

program. This application uses the finite element method (FEM). Therefore, it was possible to refine the mesh (triangular type) in the wall area. In the case of the FDTD method, the mesh was uniform in the entire area and the Yee cell size was 0.5 mm. The differences between the models, using both numerical methods, were up to 2%. The reason could be the specificity of the methods and the mesh used.

At the frequency f = 2.4 GHz, with low concrete loss, the material with the highest relative permittivity ε_r' = 8 showed comparable values to concrete ε_r' = 7. However, at the frequency f = 5 GHz, the highest field values were found for ε_r' = 5. At low–medium attenuation, the effects of wave interference resulting from wave propagation in an inhomogeneous medium and the associated partial wave reflection at the air–wall and wall–air boundaries are of fundamental importance. For 5 GHz, the results for the model with ε_r' = 7 were similar to the characteristics for ε_r' = 5. For a concrete wall with ε_r' = 7, at a higher frequency (f = 5 GHz), the field intensity decreased by as much as approximately 40%. Higher values of ε_r' resulted in an increase in max(E_z) at a very low conductivity value. It can be stated that the electric field intensity values were comparable for each of the ε_r' values. For concrete with ε_r' = 7, both for 2.4 GHz and 5 GHz, the field values were similar. In the case of other values of electric permittivity, when comparing both frequencies, there were small differences only in the conductivity range of 0–0.3 S/m.

When comparing the results, it can be stated that, at conductivity greater than 0.1 S/m, all characteristics showed a similar course, and the change in frequency did not affect the relative values of the E_z component. For the considered concrete variants, the field intensity values reached differences not exceeding 8% at σ > 0.04 S/m. Differences greater than 8% (up to 27%) in the electric field values occurred for a wall composed of concrete, as a low-loss material, σ < 0.04 S/m, and with relative electric permittivity $\varepsilon_r'\in\{5, 8\}$. At 2.4 GHz, the models with ε_r' = 7 and σ = 0.03 S/m yielded identical maximum values for the E_z component as for the values of ε_r' and σ given by other authors [30,36,38]. Moreover, at this frequency, at ε_r' = 8, none of the considered values of conductivity yielded electric field intensity results that were analogous, in terms of the nature of the occurring field phenomena, to the solutions obtained for $\varepsilon_r'\in\{5, 6, 7\}$. At a higher frequency, regardless of the analyzed value of the relative electric permittivity $\varepsilon_r'\in\{5, 6, 7, 8\}$, the same maximum values of the E_z component were obtained at σ = 0.04 S/m.

Figure 5 shows a comparison of the instantaneous distributions of the observed field component for different values of the electric permittivity of concrete. These figures were obtained for the steady state and at the same value of conductivity. It can be seen that the wave front is not distorted because the concrete is treated as a homogeneous material. As ε_r' increases, the wavelength inside the wall decreases. Therefore, more EM wavelengths occur inside the wall at a higher electric permittivity value. Due to this, it is possible to increase the number of reflections at the interface of the media, which can result in higher values of the field intensity in the area behind the wall. This is confirmed in the figures for a low conductivity value.

Figures 7–10 show the instantaneous values of the field intensity for a wall composed of concrete at different values of ε_r' but at a constant σ = 0.00195 S/m. Successive moments of time from the point at which the plane wave approaches the wall to the passage of the EM wave through the wall are shown. Based on the figures, it can be seen that, regardless of the value of the electric permittivity, the field values do not change in the area in front of the wall, and the wavelength is not changed as a result of reflections inside the wall. The changes in the image are visible in the wall and after the EM wave has passed through the wall. The phenomenon described above is also confirmed in these figures. In the area behind the wall, due to the increase in ε_r' and the extension of the path inside the wall, with the increase in ε_r' for concrete, a delay in the passage of the wave through the wall is visible. When comparing the model with ε_r' = 5 and ε_r' = 7, the difference is one wavelength.
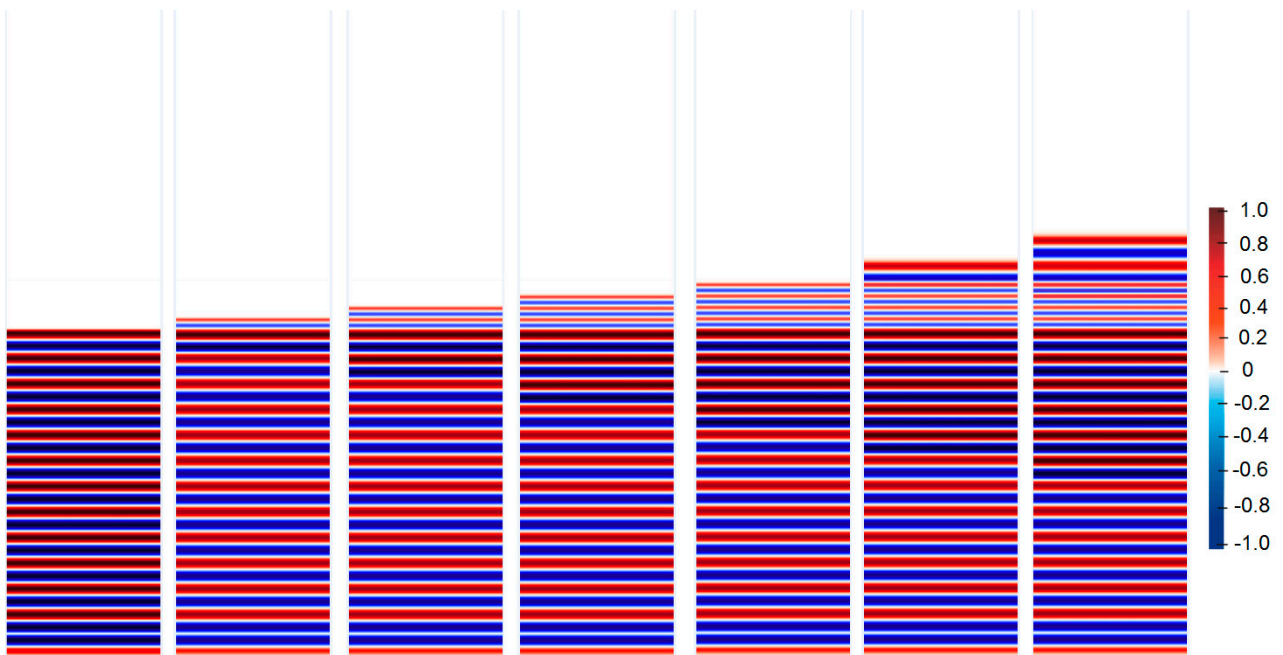
Figure 7. Propagation of EM wave through a concrete wall with the following parameters: $\varepsilon_r' = 5$ i $\sigma = 0.00195$ S/m.
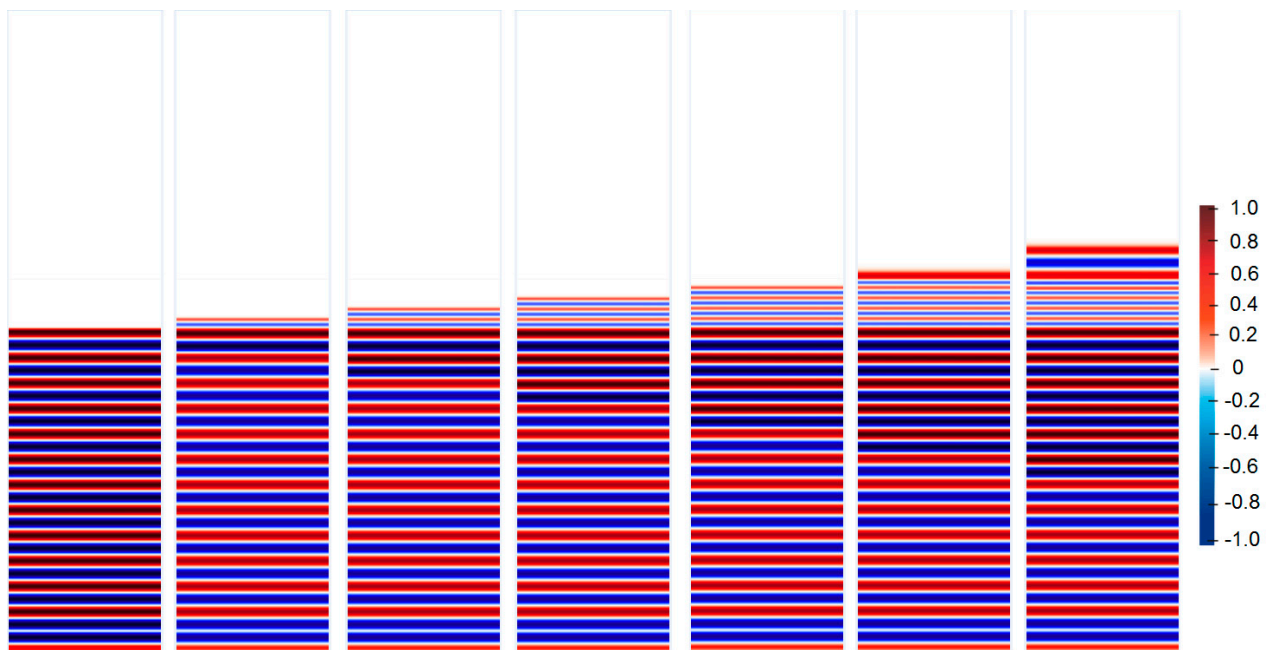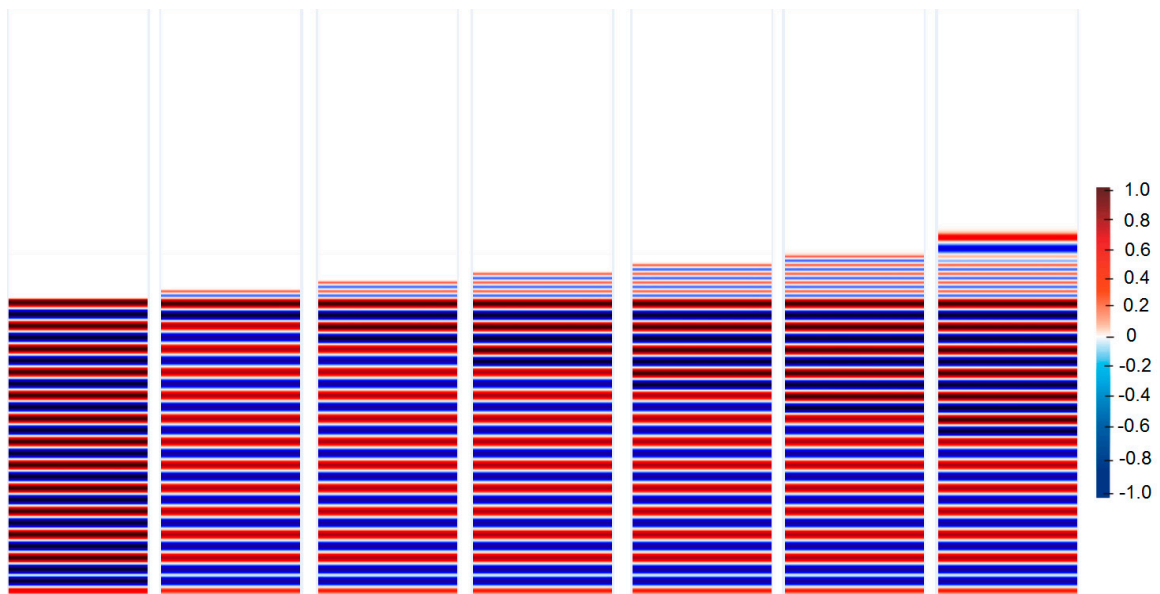

Figure 8. Propagation of EM wave through a concrete wall with the following parameters: $\varepsilon_r' = 6$ i $\sigma = 0.00195$ S/m.

Figure 9. Propagation of EM wave through a concrete wall with the following parameters: $\varepsilon_r' = 7$ i $\sigma = 0.00195$ S/m.
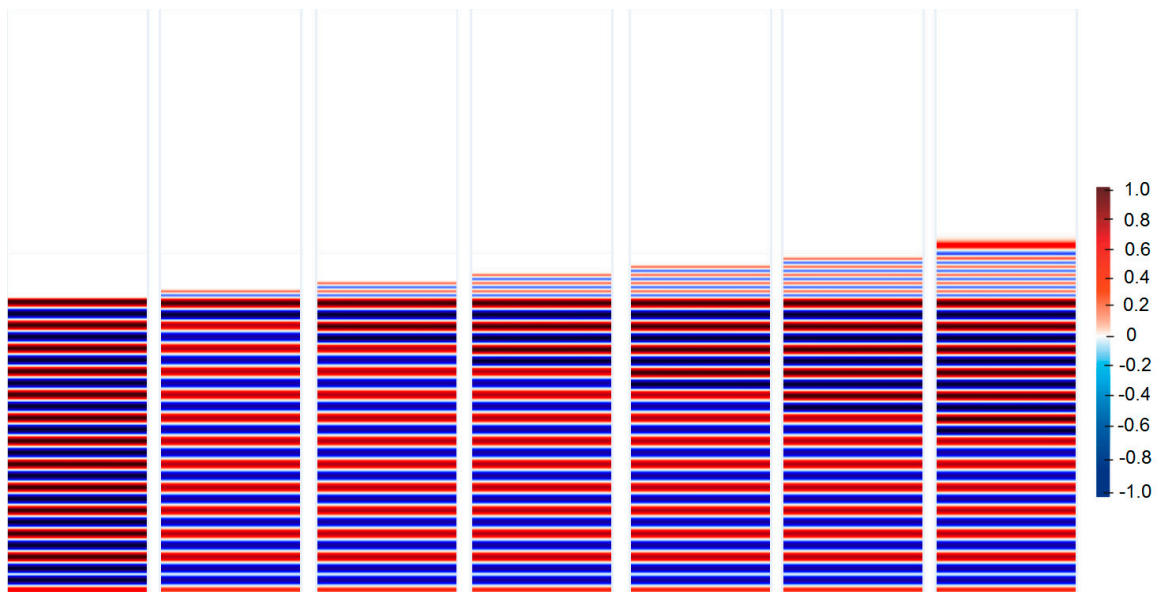

Figure 10. Propagation of EM wave through a concrete wall with the following parameters: $\varepsilon_r' = 8$ i $\sigma = 0.00195$ S/m.

5.2. Analysis of a Wall Composed of Concrete with Reinforcement

In Section 5.1, homogeneous walls composed of concrete only at different electric permittivity and conductivity values are analyzed in detail. In this section, we analyze not only the influence of parameters related to the concrete but also the number and diameter of the reinforced bars, as well as the number of rows and the spacing between the bars, at a frequency of 2.4 GHz. Due to the construction of the reinforced concrete walls, the evaluation of the phenomena in these systems was performed using the FDTD method. Figures 11 and 12 show the instantaneous distributions of the electric field at successive times for two exemplary models with one row of bars of 0.01 m diameter but with different bar spacing values, i.e., $L = 0.15$ m and $L = 0.20$ m. In both variants, the EM wave front is distorted after passing through the wall. In the case of the model with $L = 0.20$ m, these

distortions are less orderly and less symmetrical than in the model with less frequent bar spacing. Moreover, the wall model with $L = 0.20$ m causes larger distortions, with numerous momentary minima and maxima, both in the wall itself and in front of the wall. Such significant changes are not visible in the model with smaller spacing among the rods. On this basis, it is possible to conclude that larger spacing between the rods results in less predictable effects related to EM wave propagation and may cause momentary problems with wireless communication.
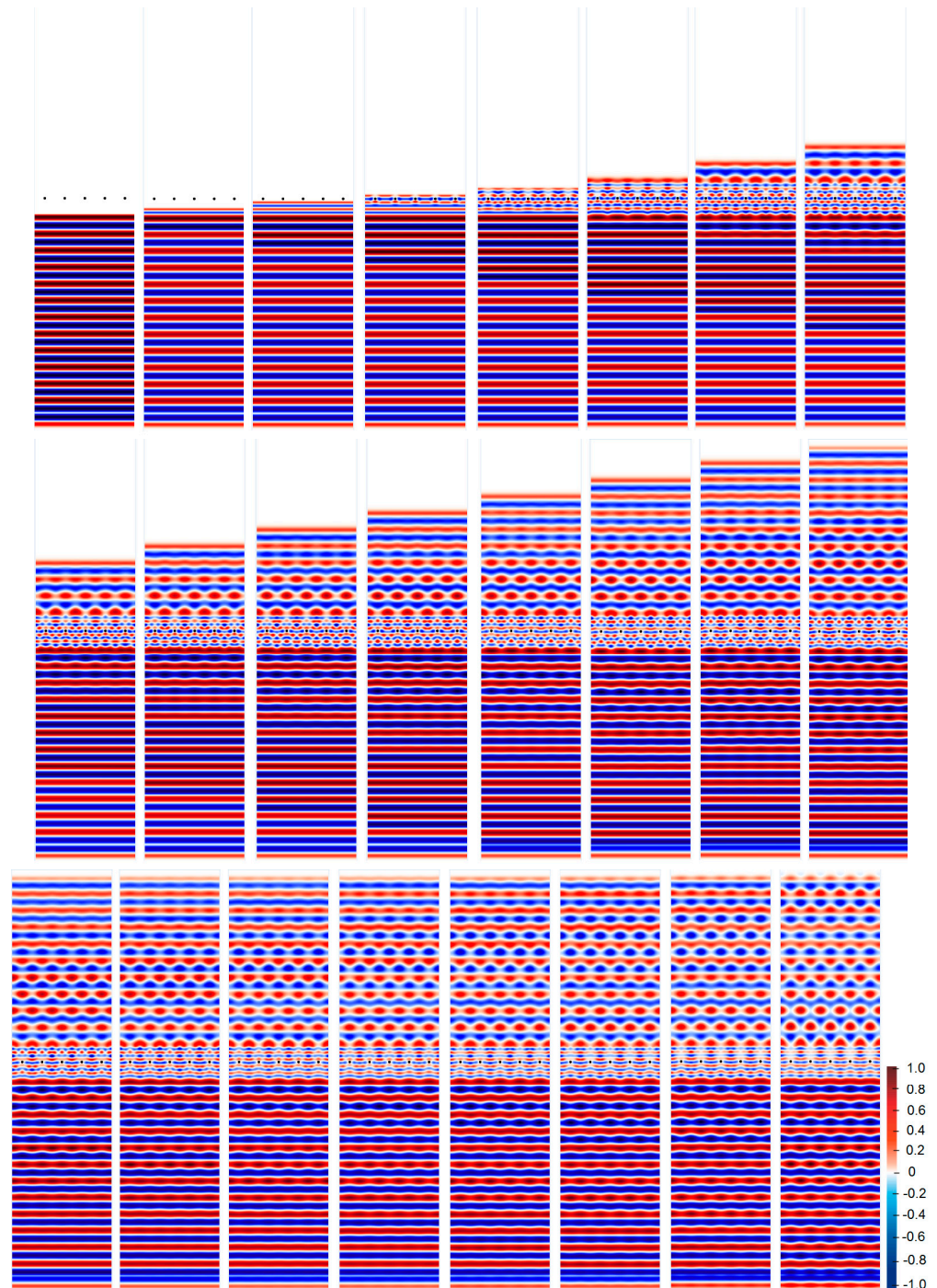
Figure 11. EM wave propagation in successive steps through a reinforced concrete wall (*fi* = 0.01 m, $L = 0.15$ m) with the parameters $\varepsilon_r' = 6$ and $\sigma = 0.00195$ S/m for the frequency of 2.4 GHz.
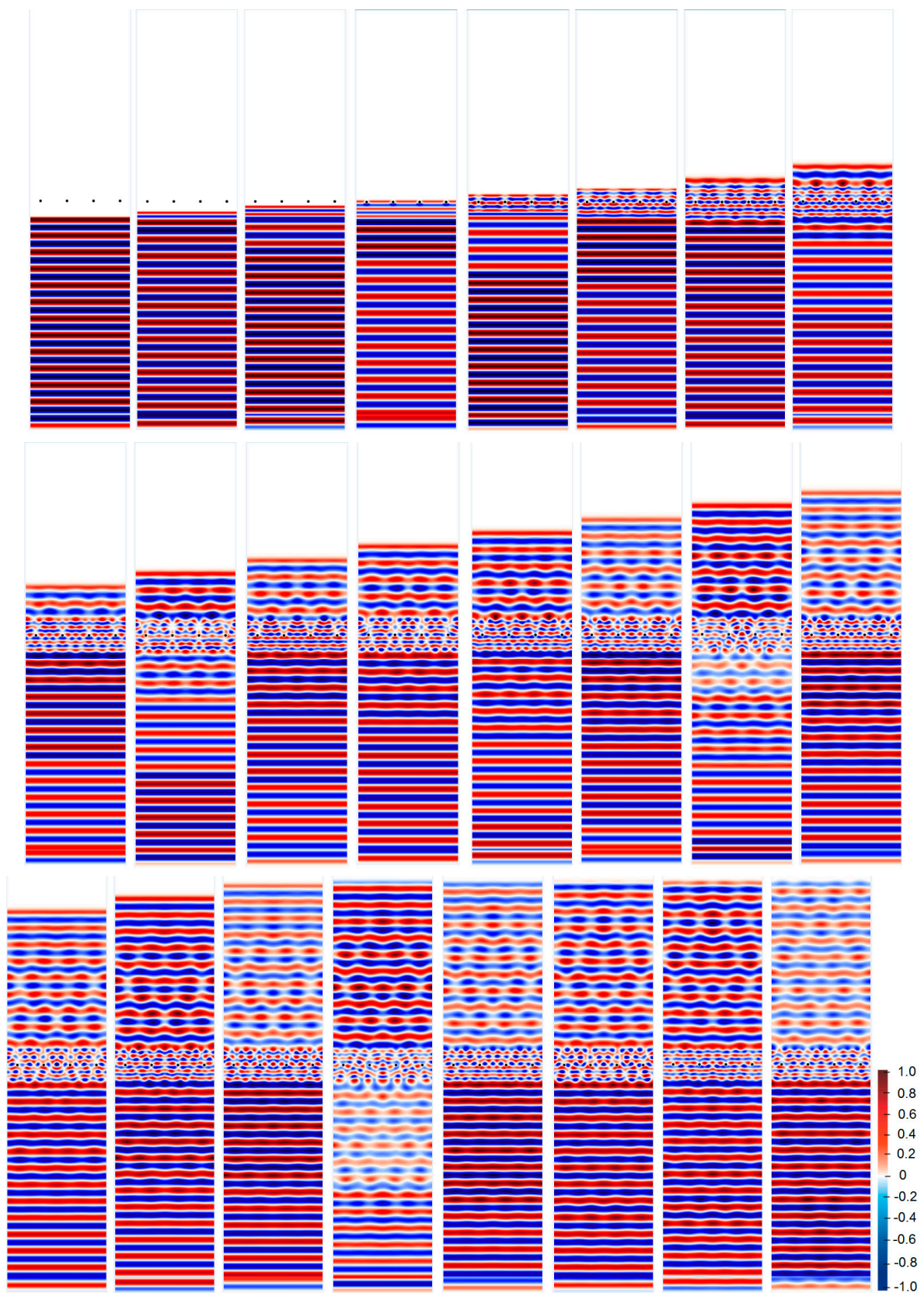
Figure 12. EM wave propagation in successive steps through a reinforced concrete wall (fi = 0.01 m, L = 0.2 m) with the parameters ε_r' = 6 and σ = 0.00195 S/m for the frequency of 2.4 GHz.

Figures 13–16 show the influence of the reinforcement diameter on the max(E_z), with the three most commonly used conductivity values. Below are the results for the four models considered, taking into account the change in the number of bar rows and the spacing between the bars constituting the reinforcement of the structure.

The analysis shows that larger spacing between the bars causes an increase in the max(E_z) in the area behind the wall; however, this relationship is not fulfilled for the relative electric permittivity of concrete $\varepsilon_r' = 5$, where, in some areas, model 1b_L15 even shows 5% higher field values than the other variants. It was also noticed that, at $\varepsilon_r' \in \{6, 7, 8\}$, the models containing one row of bars and with $L = 0.2$ m, for all analyzed reinforcement diameters, showed higher max(E_z) values—by, at most, 60%—compared to the variants with two rows of bars, which caused an increase in the number of reflections occurring at the boundaries of the media and a decrease in the effective area of electromagnetic wave attenuation. On the other hand, the models with two rows of bars and spacing $L = 0.15$ m, regardless of the reinforcement diameter, were characterized by 65% lower values of the electric field intensity compared to variants with one row of bars. In general, increasing the reinforcing bars *fi* in the range used in Europe does not significantly affect the field values; the differences amount to, at most, 4%.
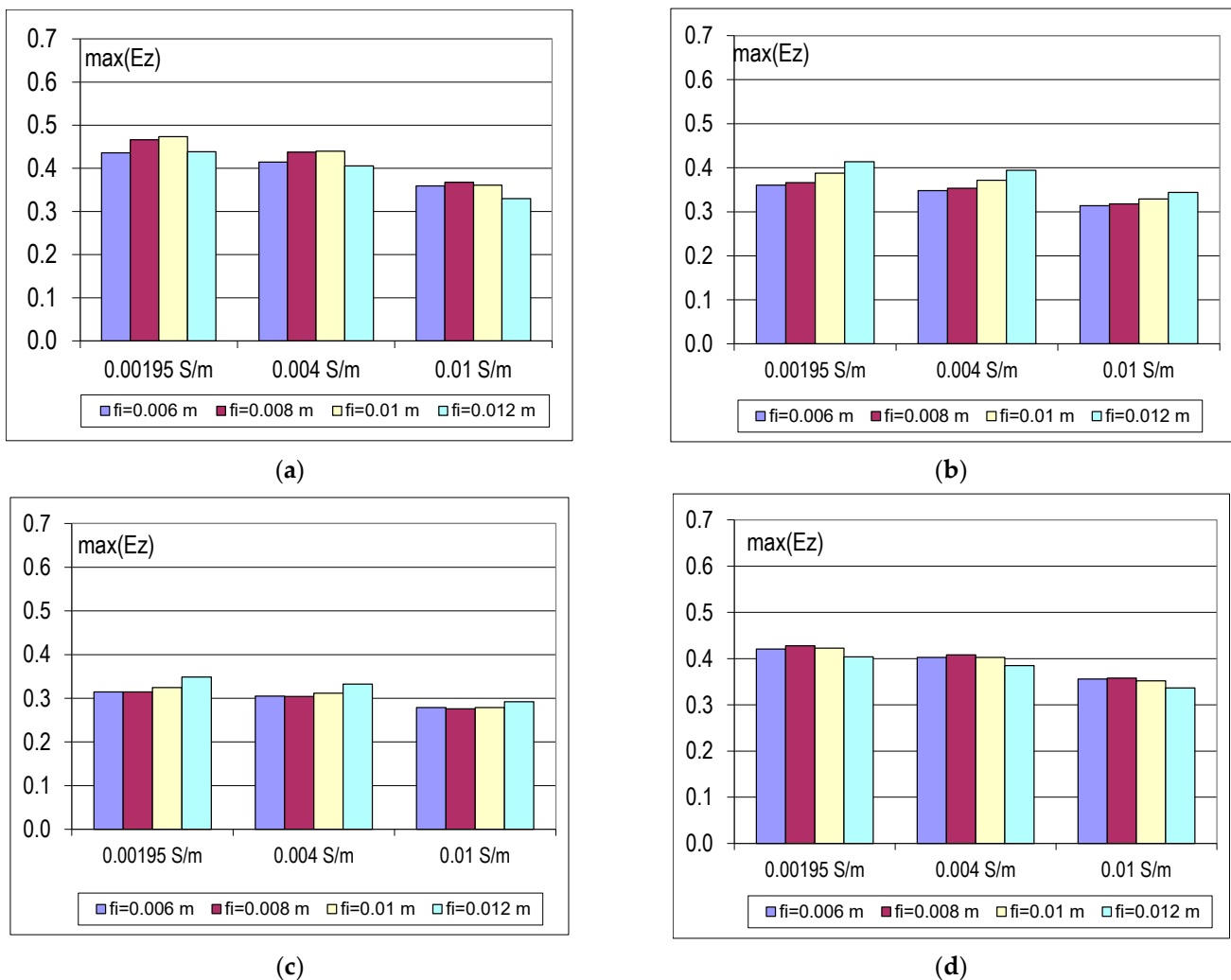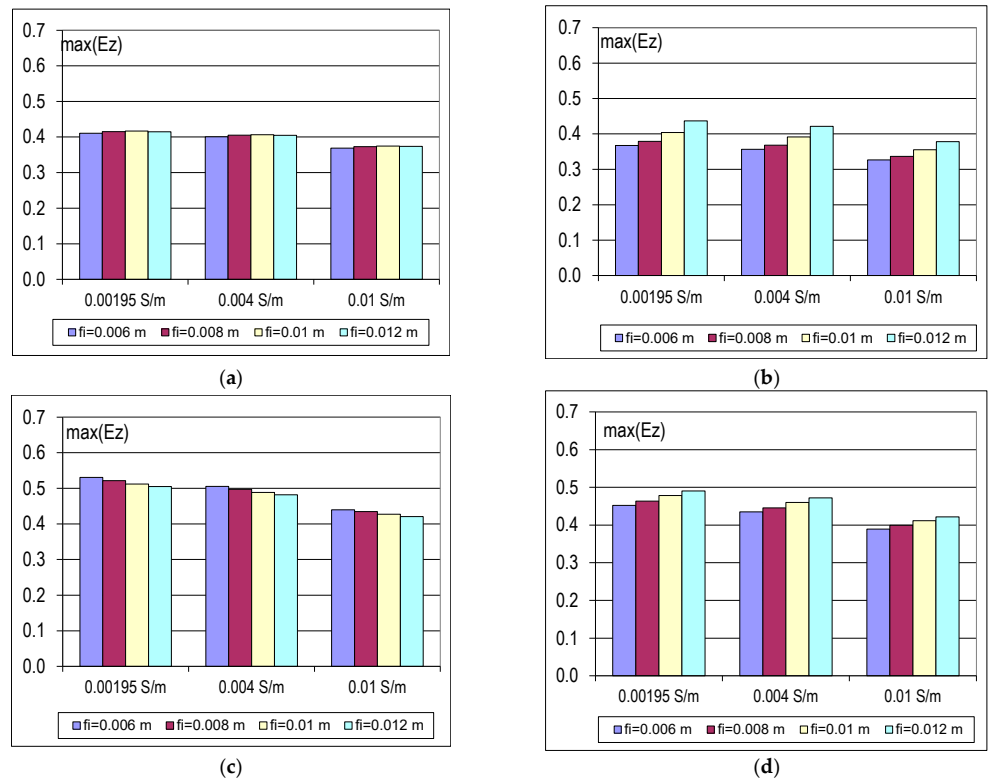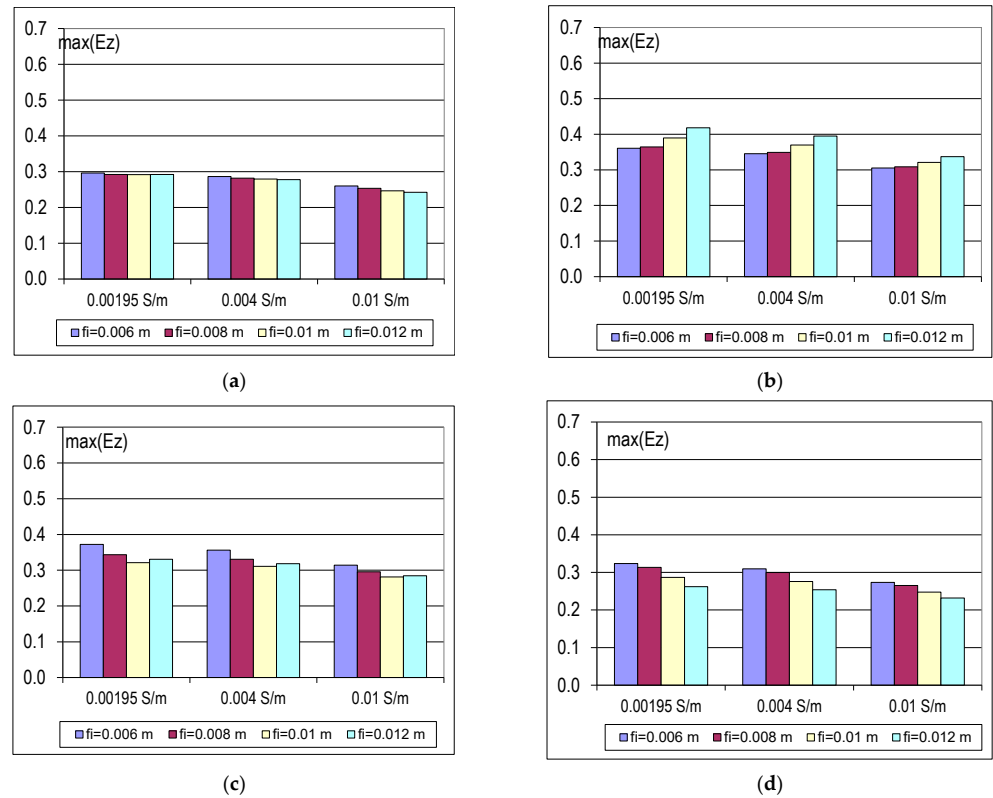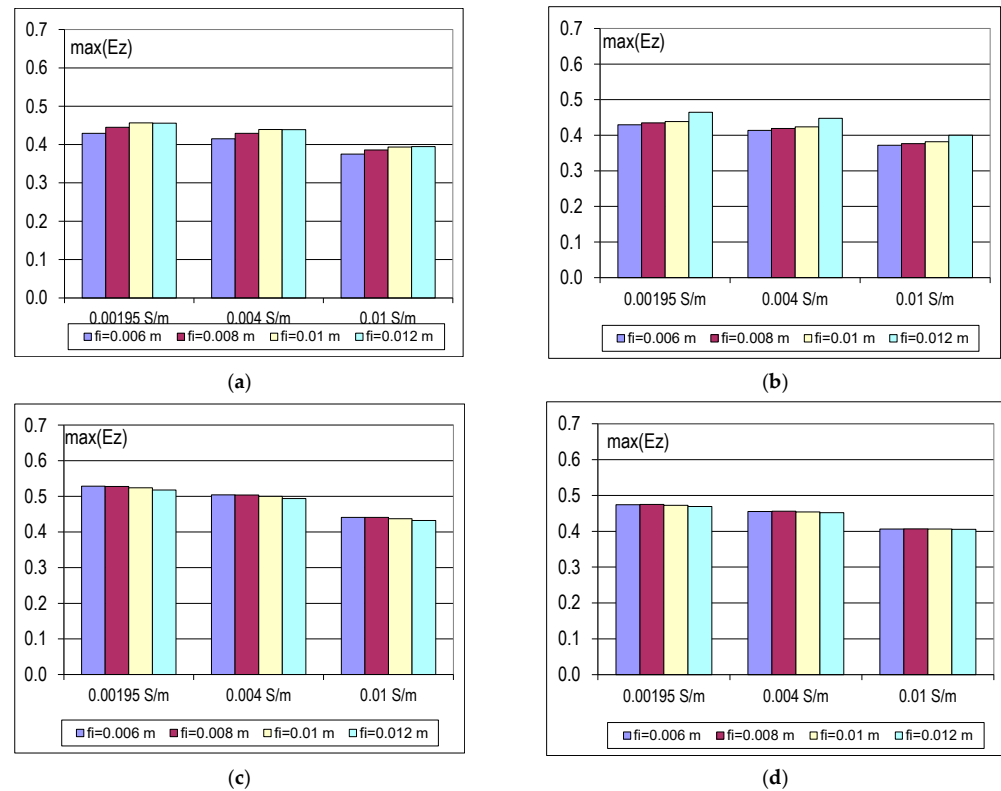

(a)

(b)

(c)

(d)

Figure 13. Relationship between reinforcement diameter and max(E_z), at different conductivity values, for model 1b_L15 and concrete with ε_r': (**a**) 5, (**b**) 6, (**c**) 7, (**d**) 8.

Figure 14. Relationship between reinforcement diameter and max(E_z), at different conductivity values, for model 1b_L20 and concrete with ε_r': (**a**) 5, (**b**) 6, (**c**) 7, (**d**) 8.

Figure 15. Relationship between reinforcement diameter and max(E_z), at different conductivity values, for model 2b_L15 and concrete with ε_r': (**a**) 5, (**b**) 6, (**c**) 7, (**d**) 8.

(**a**)

(**b**)

(**c**)

(**d**)

Figure 16. Relationship between reinforcement diameter and max(E_z), at different conductivity values, for model 2b_L20 and concrete with ε_r': (**a**) 5, (**b**) 6, (**c**) 7, (**d**) 8.

6. Results Summary

Based on the multivariate analysis, it is noted that a small change in the value of the electric permittivity of concrete above 0.04 S/m has less significance regarding the correctness of the results. However, with lower losses of concrete, at 2.4 GHz, the differences are in the order of up to 15%. Greater differences are observed at a higher frequency (up to 30%).

An analysis of systems with a wall composed of concrete, regardless of the assumed value of the electric permittivity ε_r' (i.e., 5, 6, 7, 8), showed that, in the case of the frequency of 2.4 GHz with higher concrete losses (above 0.9 S/m), the characteristics exhibited a similar course. However, at 5 GHz and above 0.03 S/m, the field intensity values are similar and differ only by an average of 5%. The largest field discrepancies are observed at 2.4 GHz and below 0.3 S/m.

When analyzing reinforced concrete walls, the conclusions were more complex. The reason was the presence of steel rods in the structure, which led to numerous reflections and interferences due to waves. The effect consisted of momentary disappearances and amplifications of the field values. When analyzing the maximum values of the field behind the wall, the following conclusions were obtained.

1. In models with a single row of bars, doubling the distance between the bars results in higher field values.

    ○ The largest increase is for $\varepsilon_r' = 7$ and $\sigma = 0.00195$ S/m and amounts to about 40%.
    ○ However, for $\varepsilon_r' = 5$, the situation is reversed and the field values are higher for a denser mesh ($L = 0.15$ m), by a maximum of approximately 5%.
    ○ At $\varepsilon_r' = 6$, the field values are comparable for two distances between the bars.

2. In the models with two rows of bars, doubling the distance between the bars also results in higher field values, regardless of ε_r'. Compared to the model with one row of bars, the values are significantly higher.

    ○ The highest field strength increases are at $\varepsilon_r' = 5$ and $\varepsilon_r' = 8$ (up to 50%).

    ○   The lowest field value increases are at $\varepsilon_r' = 6$ (approx. 12%).

3. In most models, the electric field values decrease with the increase in the reinforcement diameter. The exceptions are models with one row of bars at $L = 0.2$ m for $\varepsilon_r' = 6$ and $\varepsilon_r' = 8$.

4. Regardless of the model, reducing the conductivity value, the diameter of the bars, and the electric permittivity results in a decrease in the electric field value. The greatest differences are visible for $\varepsilon_r' = 7$ in the model with one bar and larger spacing between the bars. For example, a tenfold increase in the loss of concrete causes a decrease in the field by about 15%.

The above conclusions show that models of walls or structures containing reinforced concrete must be considered individually. Using the above-mentioned main observations as an example, it can be seen that there are exceptions that indicate the occurrence of numerous physical phenomena that significantly affect wave propagation and the signal quality. Figure 17 presents the aggregated results for selected values that are most frequently used by other authors. It was found that, at the spacing of $L = 0.15$ m, doubling the number of reinforcement rows significantly reduces the electric field intensity values by up to 40%. An exception was the case with $\varepsilon_r' = 6$, $\sigma = 0.00195$ S/m, where a 1% increase in the electric field value was observed.
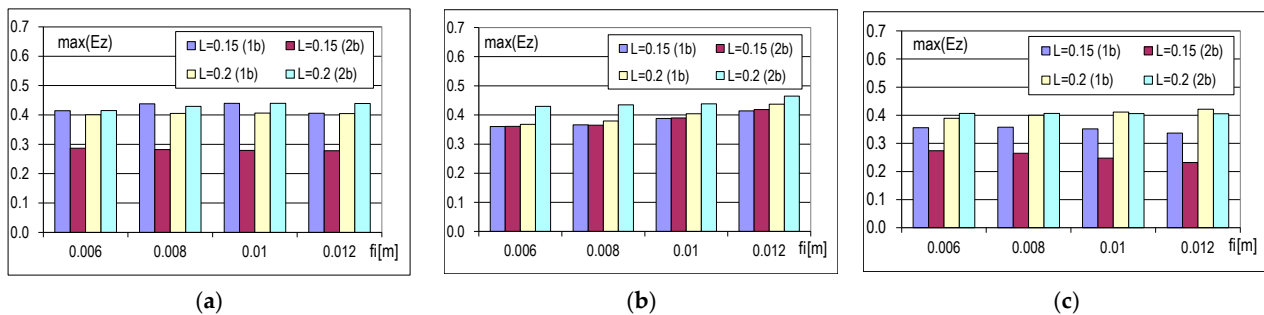

(a)   (b)   (c)

Figure 17. Relationship between reinforcement diameter and max(E_z) values for four reinforced concrete wall models calculated with typical concrete parameters: (**a**) $\varepsilon_r' = 5$ and $\sigma = 0.004$ S/m, (**b**) $\varepsilon_r' = 6$ and $\sigma = 0.00195$ S/m, (**c**) $\varepsilon_r' = 8$ and $\sigma = 0.01$ S/m.

7. Conclusions

The FDTD method was used in the calculations in this study. During the model building and tests, limitations of this method were noticed. The most significant ones included the necessity to build a rectangular grid, which limited the accurate reproduction of the model. When introducing the reinforcement, it was also necessary to adjust the grid to the diameter of the bars. Unfortunately, this method does not offer the possibility of using adaptive grids, which would allow for a significant reduction in the number of unknowns. In comparison with the frequency method, e.g., FDFD, it is necessary to obtain a steady state in order to obtain results. However, thanks to the possibility of obtaining momentary images of the field, it is possible to better understand how the EM wave propagates and where momentary signal amplifications and decays occur. The best solution would be to develop a hybrid method, which would allow for time savings during the calculations and offer the possibility of using adaptive grids.

Based on the analysis performed, it can be stated that routers should not be located near reinforced concrete walls. A homogeneous material does not cause such large changes in the EM wave front. Any non-homogeneous material that contains metal inserts, e.g., in the form of reinforcement, has a negative impact on wireless communication. For example, in a room behind a reinforced concrete wall, temporary signal loss or even no signal is possible. This depends on the amount and diameter of the reinforcement. In the case of ceilings that contain even more reinforcement, it is not advisable to mount routers close

to these structures. In this case, even greater interference would occur, which could be observed using numerical methods.

The next goal of the present authors is to investigate the influence of concrete containing metal elements (fiber concrete) and compare the results with those obtained for reinforced concrete. This new construction technology will appear more often in structures. It is similar to the modern technique of building with ceramics, where bricks and hollow blocks are used. This is a heterogeneous material that also contains air hollows and sometimes even metal inserts. Further research will focus on a thorough understanding of the physical phenomena associated with various structures. The collected database of results and conclusions will allow for the more precise planning of the locations of access points or routers. It is not possible change the construction of the wall, but, using the collected knowledge, we can improve the signal quality.

Author Contributions: The paper was written by A.C. The methodology was developed by A.C. The validation was performed by T.S., D.K. and A.J. The analysis was performed by A.C. The investigation was carried out by A.C. The results presented in this paper were obtained by A.C. The resources were gathered by A.C., T.S., D.K. and A.J. The review, editing and improvements to the content were performed by A.C., T.S. and D.K. Funding acquisition was performed by T.S., D.K. and A.J. All authors have read and agreed to the published version of the manuscript.

Data Availability Statement: The original contributions presented in this study are included in the article. Further inquiries can be directed to the corresponding author.

Conflicts of Interest: The authors declare no conflicts of interest.

References

1. Ye, Z.; Wang, Y.; Shao, Y. The Characteristic Research of Electromagnetic Wave Propagation in the Building. In Proceedings of the 2018 International Conference on Microwave and Millimeter Wave Technology (ICMMT), Chengdu, China, 7–11 May 2018; pp. 1–3.
2. Qin, Y.; Liu, Z.; Guo, L.; Guo, L.; Zuo, W. Research on the Influence of Changes in Building Wall Materials on the Attenuation of Radio Waves Through Walls. In Proceedings of the 2023 IEEE 11th Asia-Pacific Conference on Antennas and Propagation (APCAP), Guangzhou, China, 22–24 November 2023; pp. 1–2.
3. Asp, A.; Hentilä, T.; Valkama, M.; Pikkuvirta, J.; Hujanen, A.; Huhtinen, I. Impact of Concrete Moisture on Radio Propagation: Fundamentals and Measurements of Concrete Samples. In Proceedings of the 16th International Symposium on Wireless Communication Systems (ISWCS), Oulu, Finland, 27–30 August 2019; pp. 542–547.
4. Ferreira, D.; Cuinas, I.; Caldeirinha, R.F.S.; Fernandes, T.R. A review on the electromagnetic characterisation of building materials at micro- and millimetre wave frequencies. In Proceedings of the 8th European Conference on Antennas and Propagation (EuCAP 2014), The Hague, Netherlands, 6–11 April 2014; pp. 145–149.
5. Saito, K.; Kang, C.; Takada, J.I. Multi-Layer Building Material Modeling and Parameter Estimation Method by Wide-Band Free Space Measurement. *IEEE Access* **2024**, *12*, 67392–67404. [CrossRef]
6. Andersen, J.B.; Rappaport, T.S. In-building wideband partition loss measurements at 2.5 and 60 GHz. *IEEE Trans. Wirel. Commun.* **2004**, *3*, 922–928. [CrossRef]
7. Dalke, R.A.; Holloway Ch, L.; McKenna, P.; Johansson, M.; Ali, A.S. Effects of reinforced concrete structures on RF communications. *IEEE Trans. Electromagn. Compat.* **2000**, *42*, 486–496. [CrossRef]
8. Iskander, M.F.; Yun, Z. Propagation prediction models for wireless communications systems. *IEEE Trans. Microw. Theory Tech.* **2002**, *50*, 662–673. [CrossRef]
9. Ogunsola, A.; Reggiani, U.; Sandrolini, L. Shielding effectiveness of reinforced concrete structures. In Proceedings of the International Conference on Electromagnetic Compatibility, Phuket, Thailand, 27–29 July 2005; pp. 1A-2-1–1A-2-4.
10. Elgy, J.; Andre, D.; Morrow, I.L.; Finnis, M. Remote Determination of Building Material Characteristics Using Asymmetric Bistatic Radar Geometries. In Proceedings of the 12th European Conference on Synthetic Aperture Radar (EUSAR 2018), Aachen, Germany, 4–7 June 2018; pp. 843–846.

11. Ferreira, D.; Cuinas, I.; Caldeirinha, R.F.S.; Fernandes, T.R. Assessing Transparency Control of Southern European Building Wall Structures Using Frequency-Selective Surfaces. *IEEE Antennas Propag. Mag.* **2018**, *60*, 137–153. [CrossRef]

12. Zhekov, S.S.; Franek, O.; Pedersen, G.F. Dielectric Properties of Common Building Materials for Ultrawideband Propagation Studies [Measurements Corner]. *IEEE Antennas Propag. Mag.* **2020**, *62*, 72–81. [CrossRef]

13. Urahashi, M.; Hirata, A. Complex Permittivity Evaluation of Building Materials at 200–500 GHz Using THz-TDS. In Proceedings of the 2020 International Symposium on Antennas and Propagation (ISAP), Osaka, Japan, 25–28 January 2021; pp. 539–540.

14. Richalot, E.; Bonilla, M.; Won, M.; Fouad-Hanna, V.; Baudrand, H.; Wiart, J. Electromagnetic propagation into reinforced-concrete walls. *IEEE Trans. Microw. Theory Tech.* **2000**, *48*, 357–366. [CrossRef]

15. Rogier, H.; Zutter, D.D. A fast converging series expansion for the 2-D periodic Green's function based on perfectly matched layers. *IEEE Trans. Microw. Theory Tech.* **2004**, *52*, 1199–1206. [CrossRef]

16. Zhekov, S.S.; Nazneen, Z.; Franek, O.; Pedersen, G.F. Measurement of Attenuation by Building Structures in Cellular Network Bands. *IEEE Antennas Wirel. Propag. Lett.* **2018**, *17*, 2260–2263. [CrossRef]

17. Antonini, G.; Orlandi, A.; D'elia, S. Shielding effects of reinforced concrete structures to electromagnetic fields due to GSM and UMTS systems. *IEEE Trans. Magn.* **2003**, *39*, 1582–1585. [CrossRef]

18. Li, L.; Forsyth, R.; Jackson, C. Potential of Steel-Fibre-Reinforced Concrete to increase RFI mitigation of antenna foundations. In Proceedings of the 2013 Asia-Pacific Symposium on Electromagnetic Compatibility (APEMC), Melbourne, Australia, 20–23 May 2013; pp. 1–4.

19. Dérobert, X.; Villain, G.; Ihamouten, A. Recent developments of EM non-destructive testing in the radar frequency-band for the evaluation of cover concretes. In Proceedings of the 2015 European Radar Conference (EuRAD), Paris, France, 9–11 September 2015; pp. 233–236.

20. Paknys, R. Reflection and transmission by reinforced concrete—Numerical and asymptotic analysis. *IEEE Trans. Antennas Propag.* **2003**, *51*, 2852–2861. [CrossRef]

21. Torabi, A.; Shishegar, A.G. Scattering with reinforced concrete wall in 900 MHz band using MOM/CI method. In Proceedings of the 2009 3rd European Conference on Antennas and Propagation, Berlin, Germany, 23–27 March 2009; pp. 121–125.

22. Elkamchouchi, H.M.; Abdelkader, A.T. Shielding effectiveness of reinforced concrete structures in cellular communication bands. In Proceedings of the Nineteenth National Radio Science Conference, Alexandria, Egypt, 21 March 2002; pp. 192–199.

23. Xu, H.; Chen, Y. Simulation research on high-frequency electromagnetic plane wave's energy distribution in dielectric. In Proceedings of the 2010 2nd International Conference on Advanced Computer Control, Shenyang, China, 27–29 March 2010; pp. 321–324.

24. Weiping, Q.; Shenggao, D.; Yerong, Z. FDTD calculation of the effects of reinforced concrete wall on short path propagation of UWB pulse. In Proceedings of the 2005 Asia-Pacific Microwave Conference Proceedings, Suzhou, China, 4–7 December 2005; pp. 1–3.

25. Tanaka, S.; Begum, H. Nondestructive measurement of diameter of reinforcing bars in concrete using an electromagnetic wave radar under the effect of cross bars. In Proceedings of the SICE Annual Conference 2010, Taipei, Taiwan, 18–21 August 2010; pp. 1–6.

26. Peña, D.; Feick, R.; Hristov, H.D.; Grote, W. Measurement and modeling of propagation losses in brick and concrete walls for the 900-MHz band. *IEEE Trans. Antennas Propag.* **2003**, *51*, 31–39. [CrossRef]

27. Sołjan, Z.; Hołdyński, G.; Zajkowski, M. The mathematical concept of the currents' asymmetrical components in three-phase four-wire systems with sinusoidal and asymmetric voltage supply. *Bull. Pol. Acad. Sci. Tech. Sci.* **2019**, *67*, 271–278. [CrossRef]

28. Sołjan, Z.; Zajkowski, M.; Borusiewicz, A. Reactive Power Compensation and Distortion Power Variation Identification in Extended Budeanu Power Theory for Single-Phase Systems. *Energies* **2024**, *17*, 227. [CrossRef]

29. Stankiewicz, J.M. Comparison of the efficiency of the WPT system using circular or square planar coils. *Przegląd Elektrotechniczny* **2021**, *97*, 38–43. [CrossRef]

30. Zhang, Z.; Sorensen, R.K.; Yun, Z.; Iskander, M.F.; Harvey, J.F. A ray-tracing approach for indoor/outdoor propagation through window structures. *IEEE Trans. Antennas Propagat.* **2002**, *50*, 742–748. [CrossRef]

31. Iskander, M.F.; Yun, Z.; Zhang, Z. Outdoor/indoor propagation modeling for wireless communications systems. In Proceedings of the IEEE Antennas and Propagation Society International Symposium. 2001 Digest. Held in Conjunction with: USNC/URSI National Radio Science Meeting, Boston, MA, USA, 8–13 July 2001; Volume 2, pp. 150–153.

32. Begum, H.; Okamoto, M.; Tanaka, S. Measuring the diameter of reinforcing bars in concrete nondestructively using electromagnetic wave radar. In Proceedings of the 2008 SICE Annual Conference, Chofu, Japan, 20–22 August 2008.

33. Zhao, Z.B.; Cui, X.; Li, L.; Gao, C. Analysis of shielding performance of reinforced concrete structures using the method of moments. *IEEE Trans. Magn.* **2008**, *44*, 1474–1477. [CrossRef]

34. Van Damme, S.; Franchois, A.; Taerwe, L. Comparison of two coaxial probes for the non-destructive evaluation of a steel fiber reinforced concrete layer. In Proceedings of the 21st IEEE Instrumentation and Measurement Technology Conference, IMTC'04, Como, Italy, 18–20 May 2004; Volume 1, pp. 579–582.

35. Chiba, H.; Miyazaki, Y. Analysis of radio wave reflection and transmission characteristics at reinforced concrete slab by numerical simulation and scaled model experiment. In Proceedings of the International Symposium on Electromagnetic Compatibility, Tokyo, Japan, 17–21 May 1999; pp. 424–427.

36. Chia, M.Y.W. The effects of reinforced concrete walls/floors on wireless personal communications systems (PCS). In Proceedings of the Antennas and Propagation Society International Symposium, Newport Beach, CA, USA, 18–23 June 1995; Volume 4, pp. 1956–1959.

37. Dehmollaian, M.; Sarabandi, K. An approximate solution of scattering from reinforced concrete walls. *IEEE Trans. Antennas Propag.* **2008**, *56*, 2681–2690. [CrossRef]

38. Bungey, J.H. Sub-surface radar testing of concrete: A review. *Constr. Build. Mater.* **2004**, *18*, 1–8. [CrossRef]

39. Tanaka, S.; Wakabayashi, M. On measurement of the depth and the diameter of steel bars in reinforced concrete using electromagnetic wave (radar). In Proceedings of the SICE-ICASE International Joint Conference, Busan, Republic of Korea, 18–21 October 2006; Volume 8, pp. 2555–2559.

40. Tan, S.Y.; Tan, M.Y.; Tan, H.S. Multipath delay measurements and modeling for interfloor wireless communications. *IEEE Trans. Veh. Technol.* **2000**, *49*, 1334–1341. [CrossRef]

41. Boryssenko, A.; Boryssenko, O.; Lishchenko, A.; Prokhorenko, V. Inspection of internal structure of walls by subsurface radar. *IEEE Aerosp. Electron. Syst. Mag.* **2006**, *21*, 28–31. [CrossRef]

42. Travassos, L.; Ida, N.; Vollaire, C.; Nicolas, A. Time-Domain Modeling of Radar Assessment of Concrete: A Parametric Study; Numerical Techniques; 2008. Available online: http://www.ampere-lyon.fr/IMG/pdf/compumag1_PA6-4.pdf (accessed on 1 December 2024).

43. Wang, J.J.H. *Generalized Moment Methods in Electromagnetics, Formulation and Computer Solution of Integral Equations*; John Wiley & Sons, Inc.: Hoboken, NJ, USA, 1991.

44. Yang, M.; Stavrou, S. Three-dimensional modal transmission-line method for radio wave propagation through periodic building structures. *IEEE Proc. Microw. Antennas Propag.* **2005**, *12*, 597–603. [CrossRef]

45. Ping, L.; Gui, C.; Yun-liang, L. Effects of reinforced concrete walls on transmission of EM wave in WLAN. In Proceedings of the International Conference on Microwave and Millimeter Wave Technology, ICMMT 2008, Nanjing, China, 21–24 April 2008; Volume 1, pp. 519–522.

46. Ping, L.; Xuewang, W. The reflection and transmission properties of reinforced concrete wall. In Proceedings of the International Conference on Microwave and Millimeter Wave Technology, ICMMT'07, Guilin, China, 18–21 April 2007; pp. 1–4.

47. Kharkovsky, S.N.; Akay, M.F.; Hasar, U.C.; Atis, C.D. Measurement and monitoring of microwave reflection and transmission properties of cement-based specimens. *IEEE Trans. Instrum. Meas.* **2002**, *51*, 1210–1218. [CrossRef]

48. Pinhasi, Y.; Yahalom, A.; Petnev, S. Propagation of ultra wide-band signals in lossy dispersive media. In Proceedings of the IEEE International Conference on Microwaves, Communications, Antennas and Electronic Systems, COMCAS 2008, Tel-Aviv, Israel, 13–14 May 2008; pp. 1–10.

49. Orfanidis, S.J. Electromagnetic Waves and Antennas. Rutgers University. Available online: https://eceweb1.rutgers.edu/~orfanidi/ewa/ewa-1up.pdf (accessed on 28 October 2024).

50. Morawski, T.; Gwarek, T. *Pola i Fale Elektromagnetyczne*; WNT: Warszawa, Poland, 2017.

51. Vitucci, E.M.; Kolmonen Veli-Matti Degli-Esposti, V.; Vainikainen, P. Analysis of radio propagation in co- and cross-polarization in urban environment. In Proceedings of the IEEE 10th International Symposium on Spread Spectrum Techniques and Applications, ISSSTA'08, Bologna, Italy, 25–28 August 2008; pp. 277–281.

52. Taflove, A.; Hagness, S.C. *Computational Electrodynamics: The Finite—Difference Time—Domain Method*; Artech House: Boston, MA, USA, 2005.

53. Oskooi, A.F.; Roundyb, D.; Ibanescua, M.; Bermelc, P.; Joannopoulosa, J.D.; Johnson, S.G. MEEP: A flexible free-software package for electromagnetic simulations by the FDTD method. *Comput. Phys. Commun.* **2010**, *181*, 687–702. [CrossRef]

54. Elsherbeni, A.Z.; Demir, V. *The Finite-Difference Time-Domain Method for Electromagnetics with MATLAB Simulations*; SciTech Publishing, Inc.: Raleigh, NC, USA, 2009.

55. Dehmollaian, M.; Sarabandi, K. Hybrid FDTD and ray optics approximation for simulation of through-wall microwave imaging. In Proceedings of the IEEE Antennas and Propagation Society International Symposium, Albuquerque, NM, USA, 9–14 July 2006; Volume 7, pp. 249–252.

56. Valero, A.; Rojas, R.G. Fast analysis of electromagnetic scattering from finite strip gratings on a grounded dielectric slab. *Radio Sci.* **2000**, *35*, 1307–1314. [CrossRef]

57. Nagy, L. FDTD and ray optical methods for indoor wave propagation modeling. *Microw. Rev.* **2010**, *16*, 47–53.